Rutting Modelling of Pavement Structures, validation against Heavy Vehicle Simulator tests

Hector Mauricio Angarita Moreno

Faculty of Civil and Environmental Engineering
University of Iceland
2016

RUTTING MODELLING OF PAVEMENT STRUCTURES, VALIDATION AGAINTS HEAVY VEHICLE SIMULATOR TESTS

Hector Mauricio Angarita Moreno

30 ECTS thesis submitted in partial fulfillment of a
Magister Scientiarum degree in Civil Engineering

Advisor
Dr. Sigurdur Erlingsson
Dr. Bjarni Bessason

Faculty Representative
Dr. Thorbjörg Saevarsdottir

Faculty of Civil and Environmental Engineering
School of Engineering and Natural Sciences
University of Iceland

Reykjavik, November 2016

Rutting Modelling of Pavement Structures, validation against Heavy Vehicle Simulator tests

30 ECTS thesis submitted in partial fulfillment of a *Magister Scientiarum* degree in Civil Engineering

Faculty of Civil and Environmental Engineering
School of Engineering and Natural Sciences
University of Iceland
VR II, Hjarðarhaga 2-6
107, Reykjavik
Iceland

Telephone: 525 4000

Bibliographic information:
Hector Mauricio Angarita Moreno, 2016, *Rutting Modelling of Pavements Structures, validation against Heavy Vehicle Simulator tests*, Master's thesis, Faculty of Civil and Environmental Engineering, University of Iceland, pp 60.

Printing: Háskólaprent, Fálkagata 2. 107 Reykjavik
Reykjavik, Iceland, November 2016

Abstract

This thesis presents the analysis of three asphalt paving structures: SE14, SE18 and SE20, using the Mechanistic-Empirical (M-E) approach. The structures were tested in full scale test pits at the Swedish National Road and Transport Research Institute (VTI) and their layers were instrumented to assess the essential material parameters required to perform flexible pavement designs, M-E approach and life cycle estimation.

The two principal testing methods were the heavy vehicle simulator (HVS) and falling weight deflectometer (FWD). The leading processes used to obtain the main material parameters of each layer of the structure are the backcalculation and the comparison between measurements and calculations. The success of the methodology occurs when all graphs with measurements and calculations agree with each other.

The repeated load triaxial (RLT) test was not available to estimate the material parameters of these three structures. This thesis shows that using FWD and HVS tests can provide reasonably accurate results.

Additionally, two models are analysed and backcalculated to estimate the main parameters of the permanent deformation (PD). The two models are for unbound materials (base, subbase, subgrade) and the asphalt concrete layer.

Reliable values for main parameters of the three asphalt pavement structures (stiffness, resilient modules, k_1 and k_2) where backcalculated and the two predicting models for the degradation as a function of time show promising results when comparing mechanistic calculations and full scale test structure measurements.

Útdráttur

Í ritgerðinni er gerð grein fyrir þremur vegbyggingum, SE14, SE18 og SE20 sem prófaðar hafa verið með þungum bílhermi í hröðuðu álagsprófi á sænsku vega- og samgöngustofnuninni VTI. Í vegbyggingunum voru mælinemar er mátu svörun vegbyggingarinnar við hinu þunga umferðarálagi. Í prófununum var yfir 1 milljón yfirferða þungrar umferðar beitt og vegbyggingarnar því brotin niður. Hér var það einkum hjólfaramyndunun sem varða óásættanleg við mikinn fjölda álagsferða. Niðurstöður prófananna hafa verið greindar og samanburður er gerður við líkanreikninga er byggja á nýrri aflfræilegri greiningu. Í líkangreiningunni eru notuð tvennskonar líkön til að herma niðurbrotsferlið (hjólfaramynduninna). Sérstakt líkan var notað fyrir bikbundnu lögin og nýlegt líkan var síðan notað fyrir óbundna hluta vegarsins, þ.e. burðarlag, styrkingarlag og vegbotn. Stikar líkananna voru byggiðir á ýmsum prófunum svo sem bakreiknaðir úr falllóðsmælingum, frá plötuprófum. Einnig var stuðst við stika úr fyrri prófunum á svipuðum efnum sem finna má í heimildum.

Niðurstöðum frá prófununum og hermunanna bar nokkuð vel saman. Á það við um bæði efnislíkönin. Þróun hjólfaramyndunar úr líkanreikningunum víkja þó frá mælingum í nokkrum tilvikum þegar fjöldi yfirferða verður mikill og álagið hátt. Er það trúlega vegna þess að stikarnir sem notaðir eru í líkönunum byggja á svörun vegbyggingarinnar í upphafi prófananna og eru síðan fastar í allri greiningunni. Í raun breytast efniseiginlekarnir þegar líður á prófið vegna hugsanlegra örsprungna í malbiki sem og aukinnar þjöppunar í lögum vegbyggingarinnar. Hvernig taka á tillit til slíks er ekki einfalt mál og fyrir utan umfang þessarar ritgerðar.

Dedication

To my daughters, Evita Björk and Eyglósita, please keep smiling as you do every day.

To my parents, Saul and Leonor.

To Tatiana for showing me what is really important in this 3D realm.

Table of Contents

List of Figures

List of Tables

Notations and symbols

a – Material parameter of the proposed permanent deformation model for unbound materials (equations 8, 10 and 11).
a_1, a_2, a_3 – Regression constants related to the permanent deformation model for asphalt layer (equations 12, 13, 14 and 16).
b – Material parameter of the proposed permanent deformation model for unbound materials (equations 8, 10 and 11).
d_{max} – Maximum diameter.
E – Young's modulus of bound materials.
E_{v1} and E_{v2} – Modulus of deformation.
f_o – Frequency at reference temperature (equation 7).
h – Height.
i – Stress path number.
k_1, k_2 and k_3 – Material parameter of the k-θ model.
M_r – Resilient modulus of unbound materials.
N – Load repetitions.
N_{eq1} – Equivalent number of load cycles that yields the same permanent strain in the next stress level for the asphalt layer model.
N_i – Total number of load cycles at the end of the i^{th} stress path.
N_i^{eq} – Equivalent number of load cycles for a given stress path required to obtain the same strain accumulated in all previous stress path, for the unbound material model.
N_{i1} – Number of load cycles due to climate and loading conditions of the second season (equation 15).
p – Normal stress $(p = \frac{1}{3}(\sigma_1 + \sigma_2 + \sigma_3))$ (equation 9).
p_a – Reference pressure ($p_a = 100\ kPa$) (equation 9).
q – Deviator stress $(q = (\sigma_1 - \sigma_3))$.
S_f – Non-dimensional stress condition on the development of the permanent deformation (equation 9).
T_{ref} – Reference temperature.
V – Speed of loading in km/h.
w – Moisture content.
W_c – Water content.
z – Depth.
α – Parameter determine by regression (equation 9).
β_1 – Calibration factors.
Δt – Small time steps.
ε – Axial strain.
$\varepsilon_p(N)$ – Accumulated strain for asphalt concrete model.
ε_{p1} – First permanent strain at the end of season one for the asphalt concrete model.
ε_r – Recoverable (resilient) strain.
ε_v – Vertical strain.

$\hat{\varepsilon}_p$ – The accumulated permanent strain.
$\hat{\varepsilon}(N)$ – The accumulated permanent strain after N number of load cycles for unbound materials (equation 8).
$\hat{\varepsilon}_{pi}(N)$ – The accumulated permanent strain at the end of ith stress path after N number of load cycles for unbound materials.
$\Delta\ \varepsilon_p$ – Additional permanent strain.
θ – Bulk stress ($\theta = (\sigma_1 + 2\ \sigma_3)$).
v – Poisson's ratio.
σ – Axial stress.
σ_1, σ_2 and σ_3 – Principal stresses.
σ_d – Deviator stress ($\sigma_d = (\sigma_1 - \sigma_3)$).
τ_{oct} – Octahedral shear stress ($\tau^2_{oct} = 1/9\ ((\sigma_1 - \sigma_2)^2 + (\sigma_1 - \sigma_3)^2 + (\sigma_2 - \sigma_3)^2)$).
ω – Relaxation factor (equation 19).

Abbreviations

3D – Three dimensional.
AASHTO – American Association of State Highway and Transportation Officials.
A.C – Asphalt concrete.
APT – Accelerated pavement testing.
ASG – Asphalt strain gauges.
B.B – Bituminous binder.
B.C – Base course.
D.W – Double wheel.
ERAPAVE – Elastic Response Analysis of Pavements. A response calculation software.
FWD – Falling weight deflectometer.
HMA – Hot mix asphalt.
HVS – Heavy vehicle simulator.
M-E – Mechanistic-Empirical.
MEPDG – Mechanistic Empirical Pavement Design Guide.
MLET – Multi layer elastic theory.
PD – Permanent deformation.
RLT – Repeated load triaxial test.
S.b – Subbase.
S.g – Subgrade.
SPC – Soil pressure cell.
S.W – Single wheel.
UGM – Unbound granular material.
VTI – The Swedish National Road and Transport Research Institute.
εMU – Strain soil measuring system.

Acknowledgements

This thesis was made possible with the unconditional support and endless contribution of Dr. Sigurdur Erlingsson, always available to answer all questions raised during the development of this work.

Thanks to the University of Iceland for allowing me to combine my professional career with this Master's degree, and to all the professors from the different subjects during my Master's in the University of Iceland.

Finally, I would like to thank all the personnel at the Swedish National Road and Transport Research Institute (VTI); their contribution in performing all the testing and collection of data made possible the completion of this work.

1 Introduction

Road projects are one of the most common infrastructure activities in any country around the world. A well-developed road infrastructure provides an economic advantage to any nation in the present globalized economy. From public to private investment, the development of standards and easy tools to evaluate the flexible structure parameters and its behavior are very relevant. An extensive knowledge of parameters and models to analyse the behavior of the asphalt concrete structures provide the tools to any company or nation to make the final investment decisions on any road project.

The current design method for flexible structures rely mostly on empirical correlations with past performance, and index-values-based characterization of material properties. Factors such as constructions techniques, different subdrainage and long-term effects on pavements of climate and ageing make the empirical design approach obsolete and difficult to apply in new situations.

In the mechanistic-empirical (M-E) design method, the principles of the engineering mechanics are applied to evaluate the response of the pavement structures to traffic loading and improved prediction distresses models as a function of time. These models should be flexible to implement the new situations such as pavement materials and loading.

This study analysed three standard full scale test road structures from Sweden: SE14, SE18 and SE20. The M-E approach was used in the analysis which is very relevant as an extensive amount of testing data are available for the structures based on direct measurements in full-scale tests. For the mechanic part the main parameters were backcalculated with computational programs and models. All the material parameters are compared between the tree structures to attain the most accurate values. For the permanent deformation (PD), two relatively new empirical predicting models in literature are used to predict the final permanent deformation for the total structure.

Previous research on similar asphalt structures has been completed in recent years at the University of Iceland and the KTH Royal Institute of Technology in Sweden (Saevarsdottir, 2014; Ahmed, 2014; Rahman, 2014), just to mention a few.

1.1 Objective

The general objective of this work is to use the M-E approach to model the degradation of flexible pavement structures. This includes getting the main material parameters of the flexible structures SE14, SE18 and SE20 and obtain a better understanding of the PD as a function of time for future design and cost analysis, decision-making processes and expected time for maintenance. Additionally, this thesis puts into practice two PD models to verify its simplicity and accuracy by comparing calculation with full scale test results.

1.2 Brief chapters description

This thesis consists of five chapters. Chapter 2 gives an overview of the Mechanistic-Empirical approach. Chapter 3 provides the background theory and literature of the related work including the two essential tests: the falling weight deflectometer (FWD) and the heavy vehicle simulator (HVS), and gives a brief description of ERAPAVE, an elastic response calculation software. Chapter 4 starts with a description of the structures with its instrumentation, then the analysis of the results is presented. Chapter 5 provides the conclusions, recommendations and areas of further study.

2 The Mechanistic-Empirical (M-E) approach

A good pavement design should increase the design life, or the life expectancy of the pavement before failure. A good predicting model must consider all the variables for the design of flexible structures, for instance the subgrade, the material properties of the different layers, the geometry and number of layers, construction factors, climate and local environmental factors, the sub-drainage conditions, the traffic load, the life span expected of the structure, etc. Knowing and predicting these variables in detail is the main aim and tool of any road designer. The accuracy of these design parameters and predicting models will benefit the project in its cost and future maintenance phases.

One of the aims of this work is to use the latest models and testing procedures to predict the life span of roads, knowing as many variables and input parameters as possible. There are of course some variables which are difficult to predict and implement into de models, for example to predict the future traffic increases, environmental changes (global warming) and bad construction practices.

2.1 The flexible structure deterioration

Different types of distresses contribute to the flexible structure deterioration with the passing of time, some of them, including: rutting, fatigue cracking, material disintegration, roughness and bleeding. Those distresses at unacceptable levels will bring the pavement to fail (Mamlouk, 2006).

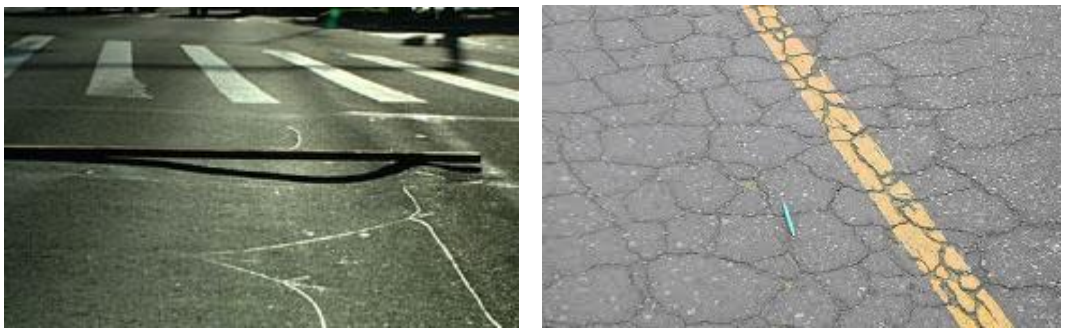

(a) (b)

Figure 2.1 (a) Rutting (b) fatigue cracking.

Rutting is the permanent deformation of the wheel path and can occur due to:

a) Unstable hot mix asphalt (HMA). This is caused by a non-optimal binder proportion, a too soft binder type, rounded aggregates, rounded texture of aggregates, or too much fine aggregates in the asphalt mix.

b) Densification of unbound aggregate layers. Due to repeat load pulses from the traffic loads the unbound layers densifies. The densification is highly aided as moisture in the layer increase.

c) Densification of HMA. This happens because of poor compaction of the HMA during the construction phase.

d) Deep settlement in the subgrade. This could happen because of a weak subgrade or bad drainage.

Fatigue cracking are a series or longitudinal interconnected cracks. The repeated loads create tensile stresses at the bottom of the asphalt layer that then create cracks. The cracks then propagate upward to the top.

Roughness is the irregularity of the pavement profile that produces uncomfortable riding.

Bleeding usually occurs during very hot weather conditions. The binder content of the HMA is then too high on the surface because it migrates upwards due to traffic loading and the softness of the binder.

Thermal cracking occurs during wintertime with the contraction of the HMA. This movement is restrained due to the friction of the underlying materials. When these tensile stresses exceed the tensile strength of the material, they develop transverse directional cracks (Mamlouk, 2006). For thin flexible pavements, rutting is the most common distress of the structure.

2.2 The Mechanistic–Empirical process

Empirical pavement design methods are usually referred to as gaining data by using the observation of the past with modifications based on laboratory performance. In pavement engineering, the empirical methods were the first steps of this evolving science. The main problem of the purely empirical methods arrives when new roads are planned with different material sources, traffic conditions, weather, etc. Applying the same material parameters to different roads in new conditions (like new materials, climate change) can imply errors in the design and extra cost during the life cycle of the road.

The engineering mechanics ensures the understanding of how the pavement structure responds to certain load conditions (Erlingsson, 2010b). Equations and models are thereafter used to predict the degradation of the structure with time. These models are also an evolving science. The new model must be simple to apply, accurate in the results, and flexible to include all variables of the pavement structure.

In the Mechanistic-Empirical approach (M-E) the main parameters of the flexible structure are obtained using the most realistic approach, recreating a mechanical model using a real

full scale pavement structure, installing instruments in many of its layers and performing the testing at a controlled climate and defined load repetitions. An extensive amount of data was received from VTI, using different temperatures and load repetitions. All the results and data are used to get high reliable parameters, using backcalculation with a software called ERAPAVE.

The benefits of the M-E approach can be summarized as follows (ARA, 2004):

- Better suited to treat the real-life environment and different wheel load conditions.
- Estimation of new load conditions.
- Better selection of materials.
- The design can incorporate the seasonal effects.
- Benefits of using adequate drainage systems.

Using the M-E approach the main parameters for stresses and strains as a function of depth, are obtained using a non-linear stress dependent model developed by ARA, (2004), which is used inside the program ERAPAVE. This model will be explained in more detail in Chapter 3.1.

Additionally, the permanent deformation (PD) of the structure is calculated using prediction models for the structure degradation as a function of time. The PD models used are relatively new in literature, and are the result of many years of research and continued evolution for the prediction of permanent deformation in bound and unbound asphalt pavement layers. These models are explained in more details in Chapter 3.2.

Figure 2.2 summarizes in a simple flow chart the M-E approach for this work.

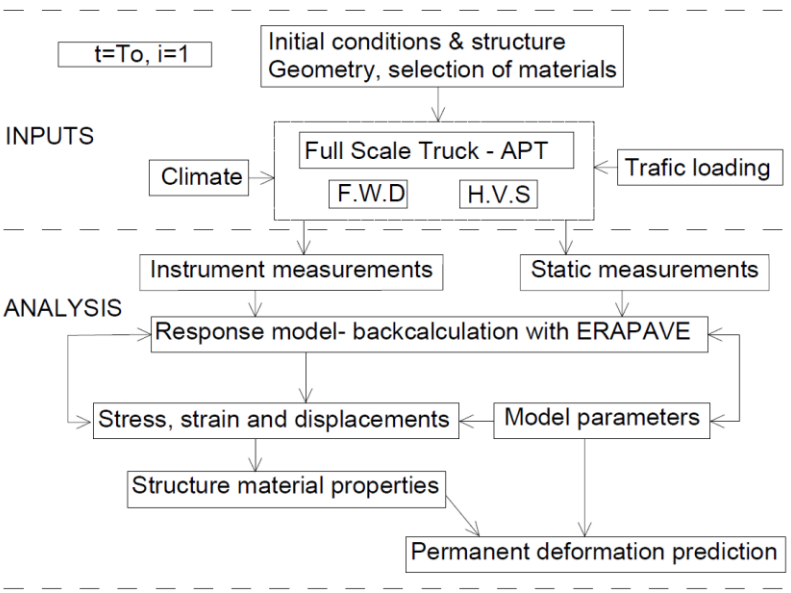

Figure 2.2 A schematic overview of the Mechanistic-Empirical model for this thesis.

In the initial part of the design i.e. t=0, all the necessary data must be collected regarding traffic, location, climate, geometry, materials, number of layers, boundary conditions, drainage, traffic loading, etc. In the full-scale test the temperature is controlled but the seasonal temperatures are one of the major impact factors for the deterioration of the asphalt concrete layers. More details of the temperature dependency of the asphalt layer are provided in Chapter 3.1.1. The traffic loading is also controlled during the HVS test, but there are many traffic variables that can affect the structure. More details of the load distribution are provided in Chapter 3.4.

The material properties of the different layers of the structure are assumed to be the same from the initial load repetitions until the end of the test. It is difficult to consider the properties changes with time and the models do not require this information for the final prediction

Finally, for the prediction of the permanent deformation as a function of time, the results of the static measurements (surface profile) are used with the support of two transfer functions models, one for the asphalt layer and the other for the unbound layers. The main parameters of the two models are again backcalculated, using the comparison of the surface profile measurements with the calculation as the main tool to provide enough confidence for the models.

3 Literature of related work

In a typical asphalt pavement structure, the applied stresses are much smaller than the strength of the materials. This means that the load does not cause the pavement to fail during one load cycle, but it may cause an infinitesimal amount of deterioration. This deterioration gradually increases with repetition of applied load cycles until unacceptable levels are reached. At this moment, the failure of the structure is considered. Different to other civil structures, the pavement is not expected to collapse (Mamlouk, 2006). The deterioration could be also influenced not only by loading, but also by different causes as described in the previous chapter.

In the structural analysis of multilayered systems as in Figure 3.1, the basic material responses of stress, strain and deformation can be estimated with relatively good accuracy. The type of load (static, moving or dynamic), the weight of the load, the material (linear or nonlinear with elastic, viscoelastic or plastic behavior) and the boundary conditions are all input parameters for the numerical solution (Mamlouk, 2006).

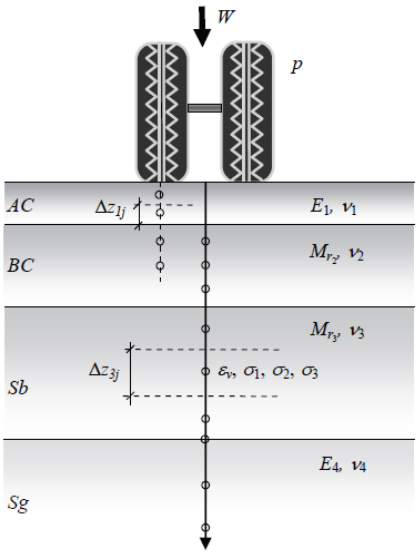

Figure 3.1 A typical road structure with its layers (Erlingsson, 2010b).

3.1 Response calculation of asphalt pavement structures

The element of a pavement structure subjected to a moving wheel can be expressed in terms of the strain. $\Delta\varepsilon_{tot} = \Delta\varepsilon_r + \Delta\varepsilon_p$. In this equation, $\Delta\varepsilon_r$ is the elastic resilient strain and $\Delta\varepsilon_p$ is the plastic strain. The Δ represents the increments during one load cycle. The elastic response contributes with the biggest portion of the total response for each load cycles so it

can be assumed that $\Delta\varepsilon_{tot} \approx \Delta\varepsilon_r$ (ARA, 2004; Erlingsson, 2010b). However, the plastic contribution accumulates with time (or number of load repetitions) and after many loading the sum of accumulated strain is $\hat{\varepsilon}_p = \sum_{i=1}^{N} \Delta\varepsilon_p$ where N is the number of load pulses applied.

The basic model by Hook's law defines the elastic material as a spring and specifies that the stress is proportional to the strain as:

$$\sigma = E \cdot \varepsilon \qquad (1)$$

where σ is stress, ε is strain and E is the Young´s modulus.

In simple words, loads are small compared to the strength of the material and after a series of repeated loads, the deformation is completely recoverable and the material can be considered elastic.

However, in reality the unbound granular layers behave as nonlinear and experience time-dependent elastoplastic responses under traffic loading (see Figure 3.2). To differentiate the nonlinear behavior from the elastic theory, the resilient response of granular materials is described with the resilient modulus M_r. Finding the appropriate M_r on a flexible structure is very critical for its design. Many factors can affect the M_r, for example the density, moisture content, aggregate sizes (fines contents and maximum sizes), aggregate type and particle shapes, load duration, frequency and load sequence (Lekarp et al., 2000a). Additionally, any variables during construction, for example the compaction during construction, the construction methods and sequence can affect the M_r. The resilient modulus of unbound materials is defined as:

$$M_r = \frac{\sigma_d}{\varepsilon_r} \qquad (2)$$

with σ_d as the deviator stress (stress in excess of the confining pressure) and ε_r is the recoverable strain (Huang, 2004).

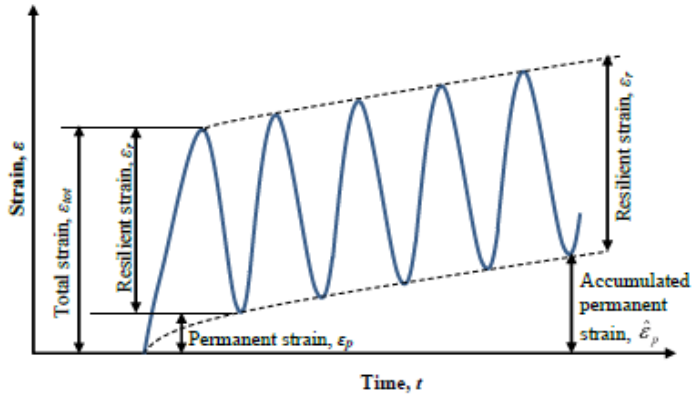

Figure 3.2 Typical strain under cyclic loading (Rahman, 2014).

The nature of the deformation has been described as the result of three main mechanisms: consolidation, distortion and attrition. Consolidation is the change in shape and compressibility of particles, the distortion mechanism is characterized by bending, sliding and rotating, and the attrition is the crushing and breaking that occurs with the application of loads (Lekarp et al., 2000a).

For the non-linear elastic materials, the k-Θ model (Seed et al., 1962; Brown and Pell, 1967; Uzan, 1992; ARA, 2004) has been used to express the stress dependency of unbound aggregate materials in terms of the bulk stress or Θ, which is the sum of the principal stress $\Theta = \sigma_1 + \sigma_2 + \sigma_2$. The hydrostatic stress is then $p = \Theta/3$.

The equation is written as follows:

$$M_r = k_1 p_a \left[\frac{\theta}{p_a} \right]^{k_2} \quad (3)$$

where the term p_a represents the reference pressure or 100 kPa and the parameters k_1 and k_2 are constants determined in a laboratory.

The model has been extended to 3D by the following expression (Uzan, 1992; Doré & Zubeck, 2009; ARA, 2004).

$$M_r = k_1 p_a \left[\frac{\theta}{p_a} \right]^{k_2} \left[\frac{\tau_{oct}}{p_a} + 1 \right]^{k_3} \quad (4)$$

where τ_{oct} is the octahedral shear stress $\tau_{oct}^2 = 1/9\,[(\sigma_1 - \sigma_2)^2 + (\sigma_1 - \sigma_3)^2 + (\sigma_2 - \sigma_3)^2]$.

Parameters k_1 and k_2 are the same as above, while k_3 is often assumed as 0 for unbound granular materials. For soils the k_3 values ranges between -0.2 to 0.0 (Erlingsson and Ahmed, 2012).

3.1.1 Temperature dependency of asphalt layer

The mechanical properties of asphalt concrete layers are heavily dependent on temperature. At low temperatures, the asphalt layer is stiff and elastic, but softens and experiences plastic behavior with increasing temperature (Oscarsson, 2007). Freeze-thaw conditions also weaken the HMA material and reduces the load capacity in all layers of the structure.

In this study the asphalt concrete layers were considered as linear elastic material and the Young´s modulus was backcalculated assuming a parameter value ranging between 5000 MPa to 7000 MPa at 10 ° C (Saevarsdottir, 2014; Ahmed, 2014; Erlingsson, 2007). The Young´s modulus was further considered as temperature dependent using the model developed by Erlingsson, (2010a).

$$E_T = E_{ref}\, e^{-b(T-Tref)} \quad (5)$$

where E_{ref} is the Young´s modulus of the bound material at reference temperature T_{ref} = 10 ° C and b = 0.05.

3.1.2 Stress dependency of unbound layers

The subbase layer consists of granular material ranging from 0 up to 90 mm in size. The base layer consists of granular material ranging from 0 mm up to 32 mm in size. Based on several studies, the unbound materials show a non-linear elastic behavior (Lekarp et al., 2000b; Uzan, 1985; May and Witczak, 1981; Huang, 1968). The model used in this study assumes the base and subbase course as stress dependent material for all the three flexible structures, see equations (3) or (4).

On the other hand, the granular subgrade composed of sand was considered as a linear elastic material. The main reason is the low stresses measured at depth in the subgrade layer reducing the non-linear behavior. This model is also in lieu with other researcher findings on the same subject (Saevarsdottir, 2014; Ahmed, 2014).

3.1.3 Asphalt Young's modulus for the HVS test

The test with the falling weight deflectometer (FWD) produce a load impulse to the pavement surface which simulates the load produce by a vehicle wheel. The speed of the falling weight used for the FWD test is fast and estimated in real time as approximately 80 km/h, while the speed of the HVS is 12 km/h (Arvidsson, 2014). To find a relationship between these two velocities and transform them into frequency, equation (6) and (7) are used (Said et al., 2013; Ahmed et al., 2013).

$$\text{Log } t = 0.5\, z - 0.2 - 0.94 \log V \tag{6}$$

$$f_o = \frac{1}{2\pi t}, \qquad a_T = \frac{f_0}{f_T} \tag{7}$$

where t [sec] is the loading time, z [m] is the depth, V [km/h] is the speed of loading, f_o [Hz] is the frequency at the reference temperature T_{ref} and f_T [Hz] is the frequency at temperature T [℃].

The master curves in Figure 3.3 were used for transforming the Young's modulus from the FWD to the HVS tests and the results are shown in Tables 4.3, 4.4 and 4.5.

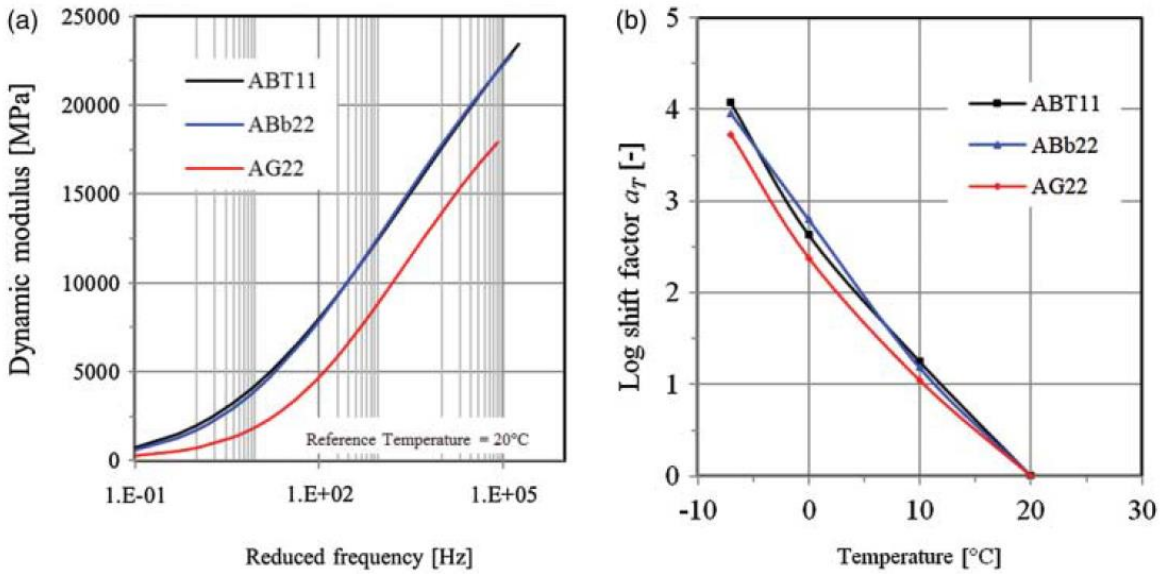

Figure 3.3 Master curves and shift factor for the dynamic modulus of ABT11, ABb22 and AG22 (Ahmed and Erlingsson, 2013).

3.2 Permanent deformation on flexible structures

Permanent deformation (PD) accumulate with time due to the applied load conditions. The increase in PD creates rutting and therefore eventual failure of the pavement structure. The development of PD is among others dependent on the stress ratio from the deviator stress and the confined pressure (Lekarp et al., 2000b).

The two typical patterns of development of PD are described in Figure 3.4.

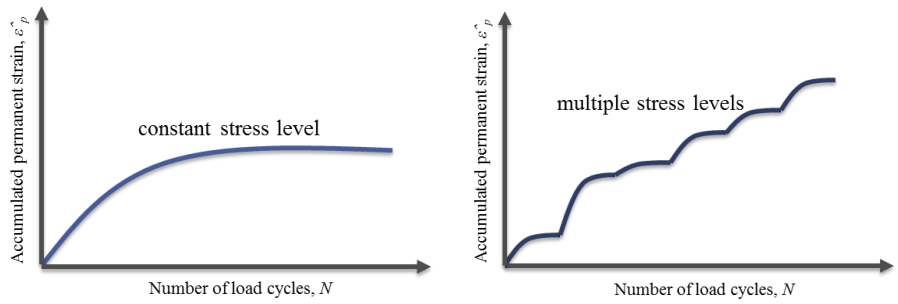

(a) (b)

Figure 3.4 (a) Accumulated strain from constant loads vs (b) Accumulated strain from variable loads (Rahman and Erlingsson, 2015).

As it will be shown in this work, the typical curve for variable accumulation of strain is common in HVS tests as the load is changed during the test for the three flexible structures.

3.2.1 Predicting model for permanent deformation of unbound materials

The predicting model used in this thesis is based on the proposed model by Sweere, (1990) and recently further developed by Rahman and Erlingsson, (2015). The model predicts the accumulation of PD in unbound materials (base and subbase layers) keeping the number of variables to a minimum. The amount of PD is dependent on the magnitude of the stresses. Additionally, the history, moisture, degree of compaction, grain size distribution and aggregate type also affect the PD (Lekarp, 1999).

The permanent strain can be classified into three types that are dependent on the stress level (Dawson and Wellner, 1999; Werkmeister et al., 2001).

In order of ascending stress levels, these are (see also Figure 3.5):

- Range A – plastic shakedown range: The post compaction is completed after many load repetitions and the material experience stabilization with no further permanent strain.

- Range B – intermediate response (plastic creep): During the first load cycles, the permanent strain rate decreases from high to low and then takes a constant permanent strain accumulation.

- Range C – incremental collapse: the permanent strain rate decreases slowly compared with A and B. A failure in accumulation of strain happens after more load applications.

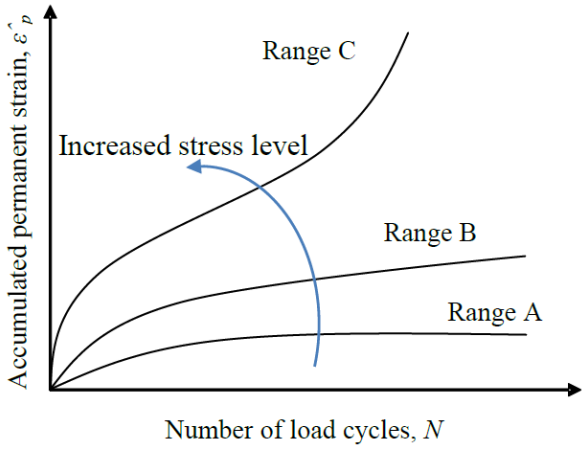

Figure 3.5 Types of PD behavior, based on stress level (Dawson and Wellner, 1999; Werkmeister et al., 2001).

The PD equation by Sweere, (1990) is a simple power law equation with few variables and it has been extended by Rahman and Erlingsson, (2015) to include stress dependency as:

$$\hat{\varepsilon}(N) = a \; N^{bS_f} \; S_f \qquad (8)$$

where $\hat{\varepsilon}(N)$ is the accumulated permanent strain after N number of load cycles, and a and b are regression parameters related to the material. The unidimensional value S_f refers to the stress condition effect on the development of PD. The S_f stress state parameter is defined as:

$$S_f = \frac{\left(\frac{q}{p_a}\right)}{\left(\frac{p}{p_a}\right)^{\alpha}} \tag{9}$$

where q is the deviator stress $(\sigma_1 - \sigma_3)$, the hydrostatic stress or normal stress is referred to as $p = \frac{1}{3}(\sigma_1 + \sigma_2 + \sigma_3)$, while α is a parameter determined by regressions and for this work the value of $\alpha = 0.75$ which is the same value proposed by Rahman and Erlingsson, (2014). P_a is the atmospheric pressure or 100 kPa to make the expression non-dimensional. The values σ_1, σ_2, *and* σ_3 are calculated using ERAPAVE at midpoint location on each of the unbound layers to be analysed.

Traffic loading includes always the lateral wander distribution (see Table 3.2) that needs to be taken into consideration, and every single lateral wander distribution has its own S_f. The final S_f value is the average of all wander distributions used in the calculation for every single layer.

3.2.2 The time hardening procedure

Asphalt pavement structures are in reality subjected to different climate and traffic conditions. The time hardening procedure by Lytton et al., (1993) combines the permanent strain contributions from different temperatures at various stress levels. For this study, the temperature will remain constant at 10˚C, but different stress paths are provided when increasing the axle load weight with the increase of the total number of load cycles.

The model in equation (8) can be extended with the time hardening approach (Rahman and Erlingsson, 2014) to include contribution from different state of stress:

$$\hat{\varepsilon}_{pi}(N) = a\ (N - N_{i-1} + N_i^{eq})^{b(S_f)_i}\ (S_f)_i \tag{10}$$

where N_i^{eq} is the equivalent number of load cycles for a given stress path, required to obtain the same amount of strain accumulated in all previous stress paths. N_i^{eq} can be calculated as:

$$N_i^{eq} = \left[\frac{\hat{\varepsilon}_{p_{i-1}}}{a(S_f)_i}\right]^{b^{-1}(S_f)_i^{-1}} \tag{11}$$

In other words, the accumulated permanent strain from the previous loading stages is used to calculate the N_i^{eq} which is required to get the same amount of strain for the new load cycle condition (Rahman and Erlingsson, 2014). The effective number of load cycles is the expression $(N - N_{i-1} + N_i^{eq})$ and this value is used for the calculation of the permanent strain during the coming stress path. The load cycle N_{i-1} is the total number of load paths at the end of the (i-1) th stress path.

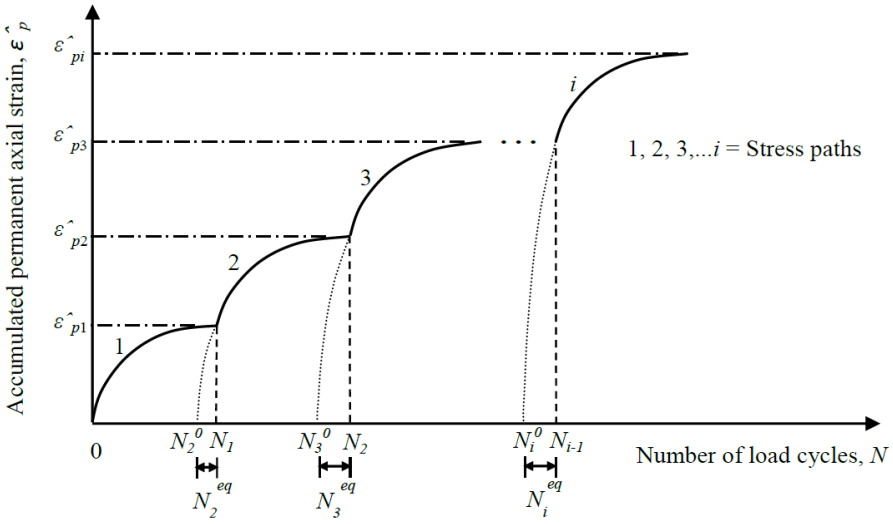

Figure 3.6 Time hardening approach scheme (Rahman and Erlingsson, 2013).

For this study, as an example of the time hardening approach, the stress levels used for pavement structure SE18 for the HVS test are given in table 3.1(Arvidsson, 2014):

Table 3.1 Stress levels used for the HVS test for structure SE18.

Load repetition	1 to 22999	23300 to 509999	510000 to 934999	935000 to 1235000
Load applied	S.W 30kN/700kPa	D.W 40kN/800kPa	D.W 50kN/800kPa	D.W 60kN/800kPa

where D.W 40kN/800kPa, means dual wheel configuration with 40kN on half-axle load with a tire pressure of 800kPa.

More details for the HVS test procedure are in chapter 3.4.

All figures shown on chapter 4.4 follows similar time hardening behavior as presented in Figure 3.6.

3.2.3 Predicting model for permanent deformation of asphalt concrete mixtures

The model developed by AASHTO under the National Cooperative Highway Research Program (NCHRP, 2004) is the one used for bound layers in this thesis because of its simplicity and the further research completed in recent years by Ahmed and Erlingsson, (2014). The equation that describes this model is:

$$\varepsilon_p(N) = \beta_1 a_1 T^{a_2} N^{a_3} \varepsilon_r \quad (12)$$

where $\varepsilon_p(N)$ is the permanent strain at N loads repetitions, β_1 is a calibration factor, T is the temperature, a_1, a_2, a_3 are regression constants and ε_r is the vertical elastic strain calculated at the middle of the layers using ERAPAVE. The lateral wander distribution in Table 3.2 is taken into consideration when calculating the $\varepsilon_p(N)$. The value for a_1 is assumed because there is no data available for the asphalt layer type ABT 16 and AG 32. On the other hand, the assumed values are taken from master curves ABT 11 and AG 22 proposed by Ahmed and Erlingsson, (2014).

The time-hardening approach by Lytton et al. (1993) is also applied to asphalt structures. Each season is characterized by a pavement temperature T_i that affects the Young's modulus, the stresses and strains of the asphalt mix.

The process starts calculating the first permanent strain at the end of season one using:

$$\varepsilon_{p1} = \beta_1 a_1 T^{a_2} N^{a_3} \varepsilon_{r1} \quad (13)$$

The equivalent number of passes N_{eq1} that will yield the same permanent strain in the next stress level must be calculated from equation (13).

$$N_{eq1} = \left(\frac{\varepsilon_{p1}}{\beta_1 a_1 T_2^{a_2} N^{a_3} \varepsilon_{r2}} \right)^{1/a_3} \quad (14)$$

To be able to use equation (14), when ε_r is negative, the values are changed to its absolute value only for the calculation of the N_{eq1}. For the final calculated value for $\Delta\varepsilon_p$ from different layers, the original negative signal was kept the same.

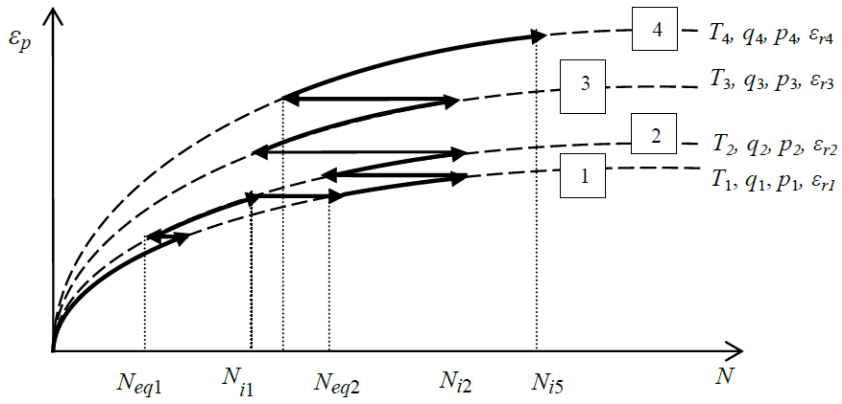

Figure 3.7 Accumulation of permanent deformation (Ahmed, 2014).

The permanent strain contribution due to the climate and loading condition of the second season is calculated from:

$$N_{i1} = N_{eq1} + \Delta N \quad (15)$$

$$\Delta\varepsilon_p = \beta_1 a_1 T_2^{a2} (N_{i1}^{a3} - N_{eq1}^{a3}) \varepsilon_{r2} \quad (16)$$

where ΔN is the number of load repetitions during the second stress condition and N_{i1} is the number of load cycles due to climate and loading conditions of the second season. Figure 3.7 shows the sequence of the model. The permanent strain at the end of the second stress condition is:

$$\varepsilon_{p2} = \varepsilon_{p1} + \Delta\, \varepsilon_p \tag{17}$$

The same procedure must be repeated until the last stress condition (Ahmed and Erlingsson, 2014).

3.3 Multilayer computational program

Different programs with different models have been developed to analyse the structural behavior and the response of flexible pavements.

The models used for these programs vary in complexity. This work selects the MLET multilayer elastic theory model because it is simple, fast and reliable (Erlingsson, 2007).

Many programs have been developed based on MLET theory, some examples include: KENLAYER (Huang, 2004), EVERSTRESS by the Washington State Department of Transportation, JULEA (Jacob Uzan Layered Elastic Analysis), and ERAPAVE (Erlingsson and Ahmed, 2012).

ERAPAVE is a software free to download and has advantages such as speedy calculations and easy to use. It has been used extensively on similar research subjects (Saevarsdottir, 2014; Ahmed, 2014).

3.3.1 ERAPAVE

Elastic Response Analysis of Pavement (ERAPAVE) is a program developed by the Swedish Road and Transportation Research Institute (VTI) for the calculation of multilayer structures. The program allows doing linear and nonlinear elastic analysis of multilayered pavements with multiple load conditions (Erlingsson and Ahmed, 2012).

Like equation (4), with the same description of its parameters, the resilient modulus follows the equation:

$$M_r = k_1 p_a \left(\frac{3p}{p_a}\right)^{k_2} \left(\frac{\tau_{oct}}{p_a} + 1\right)^{k_3} \tag{18}$$

while the resilient modulus for nonlinear layers are iterated with equation (19) (Erlingsson and Ahmed, 2012).

$$M_r^{n+1} = \omega\, M_r^n + (1 - \omega)\, k_1 p_a \left(\frac{3p}{p_a}\right)^{k_2} \left(\frac{\tau_{oct}}{p_a} + 1\right)^{k_3} \tag{19}$$

where ω is the relaxation factor.

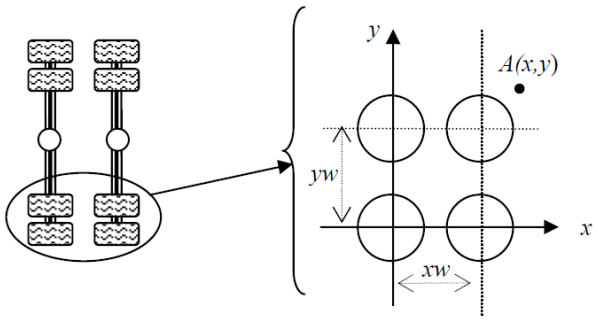

Figure 3.8 Plan view for ERAPAVE´s double wheel imprint (Erlingsson and Ahmed, 2012).

The program assumes the area under the tire to be circular (see Figure 3.8). This assumption facilitates the calculation in the program. Several studies have been done showing that the typical tire imprint is not circular and varies also depending on the type of tire (Huang, 2004), but for most practical cases a circular tire imprint has shown to give good results.

For pavement design, the contact pressure is generally assumed to be equal to the tire pressure. The contact pressure is smaller than the tire pressure for high pressure tires, because the tire surface is in tension (Huang, 2004). On the other hand, the assumption of using the same tire pressure as contact pressure represents a margin of safety for the design (Huang, 2004).

It is very important to take into consideration that many of the test data from VTI is using a coordinate system that is different to the one used for ERAPAVE. For example, for dual wheel load, usually the VTI measurement received, the origin (0,0) are given at the middle of the dual wheel, while in ERAPAVE the origin as shown in Figure 3.8 is below one of the wheels. This means a small modification on the coordinates in ERAPAVE is required to match the measurements and the results from the program.

3.4 Accelerated Pavement Testing (APT) and the Heavy Vehicle Simulator (HVS)

Accelerated Pavement Testing (APT) with a Heavy Vehicle Simulator (HVS) is a test method used to simulate pavement deterioration on a full-scale track. For this thesis the APT facility was used in conjunction with HVS and FWD to assess the asphalt pavement layers, to corroborate and validate the material parameters, to evaluate the accuracy of two models and to calculate the accumulative permanent strain of the flexible structure.

The Swedish National and transportation Research Institute (VTI) is the owner of the APT facility. All the construction of the asphalt structures, simulation, testing and data for this work was provided by them.

Figure 3.9 shows the HVS machine type Mark IV used for this test, which is the same used for almost 20 years in Sweden and Finland. It is a mobile machine which simulates the traffic loading close to real conditions. The HVS can be powered by diesel or electricity so

it is independent of external power. The unit is 23 m long, 3.7 m wide, 4.2 m high and its weight is 50 tones (Saevarsdottir et al., 2014).

Figure 3.9 HVS machine at VTI in Sweden.

A vast amount of information was collected for the three structures examined here. Single and dual wheel load were used with different load magnitudes from 30 kN to 90 kN, moving at a speed of 12 km/h. The wheel pressure was also changed between different simulation, and the range was between 500 kPa and 900 kPa. The pavement temperature can be controlled and it is set at +10˚C (Arvidsson, 2014).

The HVS test was divided into three phases: (Arvidsson, 2014)

a) A pre-loading phase is required to relieve possible residual stresses on the pavement structure. Approximately 20000 passes during one day with a single wheel of 30 kN half-axel load using an even lateral distribution with a tire pressure of 700kPa.

b) A response phase where single and dual wheel configuration was used with different types of wheel loads (40 kN, 50 kN, 65 kN half-axel) and different types of tires pressures (500 kPa, 800 kPa and 900 kPa) The response phase for SE 14 was between 20000 to 28100, for structure SE18 was 20000 to 23300 and for structure SE20 was 164800 to165000. For structure SE20 between 20000 and 164000 passes only half-axle load 40kN with 800KPa tire pressure was applied (see Table 3.2).

c) The main accelerated loading phase with more than one million load cycles applied for pavement structures SE14 and SE18 and only 745000 for pavement structure SE20. The loads are applied after the response phase with dual wheel load configuration of 40kN, 50kN and 60kN half-axle load for structures SE18 and SE20 and only 40kN and 50kN half-axle load for pavement structure SE14. The tire pressure of 800kPa was applied for all the three pavement structures.

From Table 3.2, D.W 40kN/800kPa, means dual wheel configuration with 40kN on half-axle load with a tire pressure of 800kPa.

Table 3.2 HVS load repetitions and load applied, summary table.

Pavement structure SE14

Load repetition	Load applied
1 to 19999	S.W 30kN/700kPa
20000 to 28099	Response phase
28100 to 599999	D.W 40kN/800kPa
600000 to 1204000	D.W 50kN/800kPa

Pavement structure SE18

Load repetition	Load applied
1 to 19999	S.W 30kN/700kPa
20000 to 23299	Response phase
23300 to 509999	D.W 40kN/800kPa
510000 to 934999	D.W 50kN/800kPa
935000 to 1235000	D.W 60kN/800kPa

Pavement structure SE20

Load repetition	Load applied
1 to 19999	S.W 30kN/700kPa
20000 to 164799	D.W 40kN/800kPa
164800 to 164999	Response phase
165000 to 386999	D.W 40kN/800kPa
387000 to 556999	D.W 50kN/800kPa
557000 to 745000	D.W 60kN/800kPa

The lateral wander distribution is an important condition included in the model. The wander can be modelled following a normal distribution. The values used for the normal distribution are presented in Table 3.2 (Saevarsdottir et al., 2015). The pavement structure is subjected to a traffic load that follows a normal distribution. For this reason, during testing and modelling this loading frequency must be assumed. The wander takes relevant importance when predicting the permanent deformation or permanent strain in the structure (Ahmed and Erlingsson, 2012).

Table 3.3 Lateral wander distribution for SE14, SE18 and SE20 for the main accelerated loaded test.

Position [cm]	-25	-20	-15	-10	-5	0	5	10	15	20	25
Frequency [%]	0.4	1.6	6	12	18	24	18	12	6	1.6	0.4

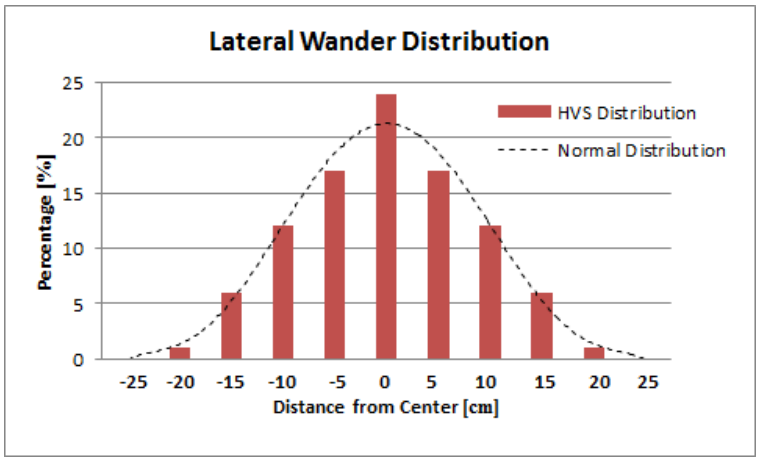

Figure 3.10 Lateral wander distribution for HVS testing.

3.4.1 Falling Weight Deflectometer (FWD)

The FWD is used as a non-destructive testing device (Figure 3.12) to measure the mechanical response of pavement structures under dynamic load. FWD is usually used as a quick and versatile testing when performing structural pavement rehabilitation and for failure detection of pavement structures (Doré & Zubeck, 2009; Huang, 2004).

The main type of analysis that can be done with the FWD are based on defection basin-shaped indicators or backcalculation of pavement layer moduli (Doré & Zubeck, 2009).

The E of the HMA and subgrade M_r parameter values for the unbound materials were not available when the HVS test started, for this reason the FWD was used to backcalculate the layer parameters of the three flexible structures.

For the location of the FWD test, the asphalt structure pit was divided into three longitudinal corridors. Each one of these corridors was tested on seven different points. Each one of these points was loaded using 30 kN, 50 kN and 65 kN applied on a circular steel plate of 30 cm in diameter. The deflections at every one of these points was measured at 0 mm, 200 mm, 300 mm, 450 mm, 600 mm, 750 mm, 900 mm and 1200 mm distance from the center of the steel plate (see Figure 3.11). An average value is selected for each corridor at different loads, to provide a unique graph.

The backcalculation involves the followings steps:

a) Input values like boundary conditions of the layers, position of deflection to be computed, densities and the load used (30 kN, 50 kN and 65 kN applied on a 30 cm circular steel plate) are entered in ERAPAVE. All tests where done before the HVS test was performed, except for structure SE20.

b) Set initial parameter data (best guess estimation) using as a reference similar layers and structures tested in the past. From literature, the vast information found on VTI web pages was used for similar pavement structures.

c) For each modulus values the program calculates deflections at 0 mm, 200 mm, 300 mm, 450 mm, 600 mm, 750 mm, 900 mm and 1200 mm.

d) Then a series of iteration approaches are required using multilayer elastic programs to finally get the best fit graph for calculated deflection vs. measured values with the minimum tolerance of error as possible (Doré & Zubeck, 2009).

All backcalculations are based on several assumptions and the most important are the linear elastic behavior of pavement and subgrade and the stress dependent analysis for the base and subbase. The ERAPAVE can calculate this assumption with minimum time consumption during the different iterations.

All the parameters and assumptions are also compared for the strain vs. depth and vertical stress vs. depth graphs. A good agreement between each load case (30 kN, 50 kN and 65 kN) for each of the structures, will provide the sufficient reliability on the parameters backcalculated.

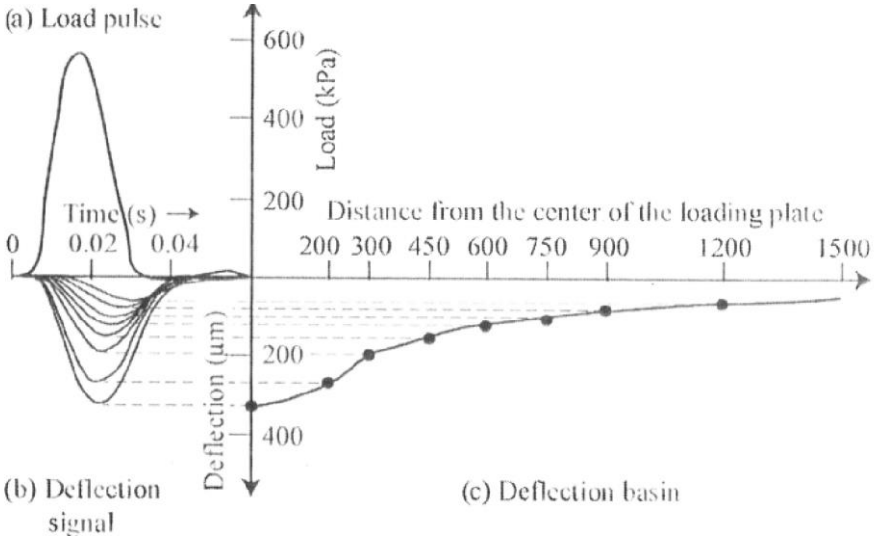

Figure 3.11 Falling weight deflectometer graph (Doré & Zubeck, 2009).

Figure 3.12 Falling weight deflectometer KUAB 50 from VTI.

4 Testing procedure and analysis of the results

The flexible structures SE14, SE18 and SE20 where constructed as full-scale pavement structures with dimensions 3 m deep, 5 m wide and 15 m long (Wiman 2006; Wiman et al., 2008). The location was Linköping Sweden in 2014 at the Swedish National Road and Transport Research Institute (VTI).

The flexible structures where equipped with instruments to compare the numerical analysis with obtained measurements. A fully detailed description of the structures with detailed gradation curves and material composition can be found in document 35-2014 of VTI (Arvidsson, 2014).

4.1 The flexible structures SE14, SE18 and SE20

The three flexible structures are briefly described below. Tables 4.1 and 4.2 summarizes the geometrical boundaries of the three structures.

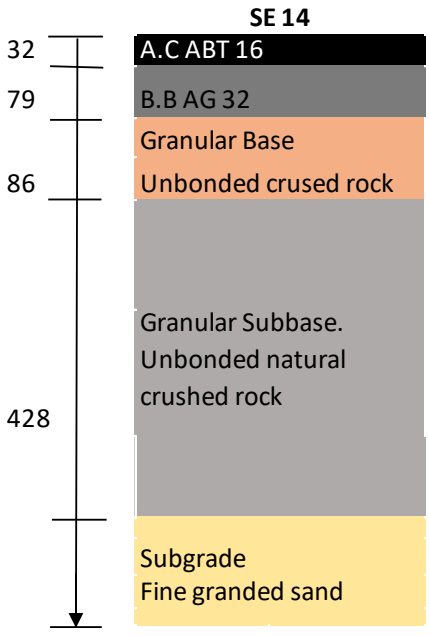

Figure 4.1 Cross section of pavement structure SE14.

The flexible structure SE14 consists of 111 mm of HMA, divided into 32 mm surface course ABT 16 (AC pen 70/100; d_{max} = 16 mm) and 79 mm of bituminous binder AG 32 (AC pen 160/220; d_{max} = 32 mm). Below the HMA there is combined crushed rock layer of total 514 mm, divided into a layer of 86 mm of unbound crushed rock with aggregate sizes between 0 to 32 mm as base course and a layer of 428 mm of unbound crushed rock with aggregate sizes of 0 to 90 mm as subbase layer. The subgrade layer is a fine graded sand material. Figure 4.1 shows the cross section of the flexible structure SE14 (Arvidsson, 2014).

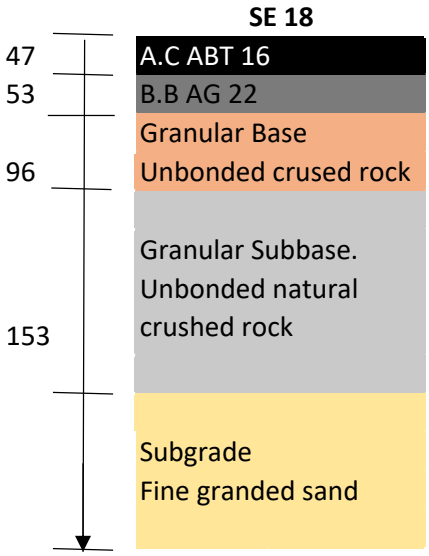

The flexible structure SE18 consists of 100 mm of HMA, divided into 47 mm surface course ABT 16 (AC pen 70/100; d_{max} = 16 mm) and 53 mm of bituminous binder AG 22 (AC pen 160/220; d_{max} = 22 mm). Below the HMA there is combined crushed rock layer of total 249 mm, divided into a layer of 96 mm of unbound crushed rock with aggregate sizes between 0 to 32 mm as base course and a layer of 153 mm of unbound crushed rock with aggregate sizes of 0 to 90 mm as subbase layer. The subgrade layer is a fine graded sand material. Below 650 mm of the structure thickness, the subgrade material from structure SE14 was used. Figure 4.2 shows the cross section of the structure SE18 (Arvidsson, 2014).

Figure 4.2 Cross section of pavement structure SE18.

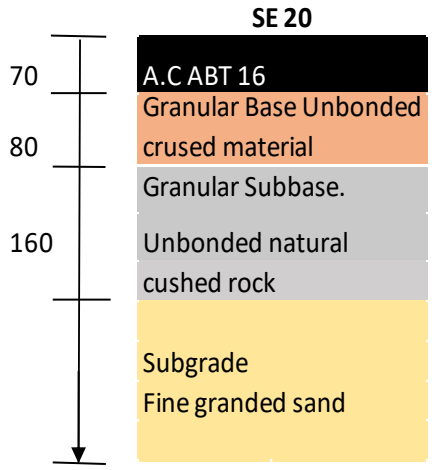

The flexible structure consists of 70 mm surface course ABT 16 (AC pen 70/100; d_{max} = 16 mm). Below the ABT there is a combined crushed rock layer of total 240 mm, divided into a layer of 80 mm of unbound crushed rock with aggregate sizes between 0 to 32 mm as base course and a layer of 160 mm of unbound crushed rock with aggregate sizes of 0 to 90 mm as subbase layer. The subgrade layer is a fine graded sand material. Below 650 mm of the structure thickness, the subgrade material from structure SE14 was used. Figure 4.3 shows the cross section of the structure SE20 (Arvidsson, 2014).

Figure 4.3 Cross section of pavement structure SE20.

Table 4.1 Summary of flexible structures SE14, SE18 and SE20 (Arvidsson, 2014).

Layer	Thickness [mm]		
	SE14	SE18	SE20
Asphalt Concrete Surface, ABT16	32	47	70
Bituminous Binder, AG32 and AG22	79	53	
Granular Base, 0-32 mm	86	96	80
Granular Subbase, 0-90mm	428	153	160
Subgrade, sand	2375	2651	2690
Total Bituminous Asphalt Structure	111	100	70
Total Base & Subbase	514	249	240
Total Structure	625	349	310

Table 4.2 Binder content of asphalt surface and bituminous layer for SE14, SE18 and SE20 (Arvidsson, 2014).

Layer	Binder content [%]		
	SE14	SE18	SE20
Asphalt Concrete Surface ABT 16 70/100	6.40	5.90	6.10
Bituminous Binder AG 22 160/220		4.20	
Bituminous Binder AG 32 160/220	4.10		

4.2 Description of instrumentation

The three structures where instrumented to measure the following parameters (see Figure 4.4):

a) The horizontal strain at the bottom of the asphalt layer using H-shaped asphalt strain gauges (ASG).

b) The vertical stress of the unbound layers using soil pressure cells (SPC).

c) The vertical strain and deformations of the unbound layers using inductive coils (εMU-coils).

d) The temperature using thermometer.

e) The PD profile was measured with laser beams.

The instrumentation and its proper installation are fundamental parts of this work. In general, good agreement was found between the different instrument measurements for the different layers of the flexible structures, and this can be validated with the graphs shown in Chapter 4.3.

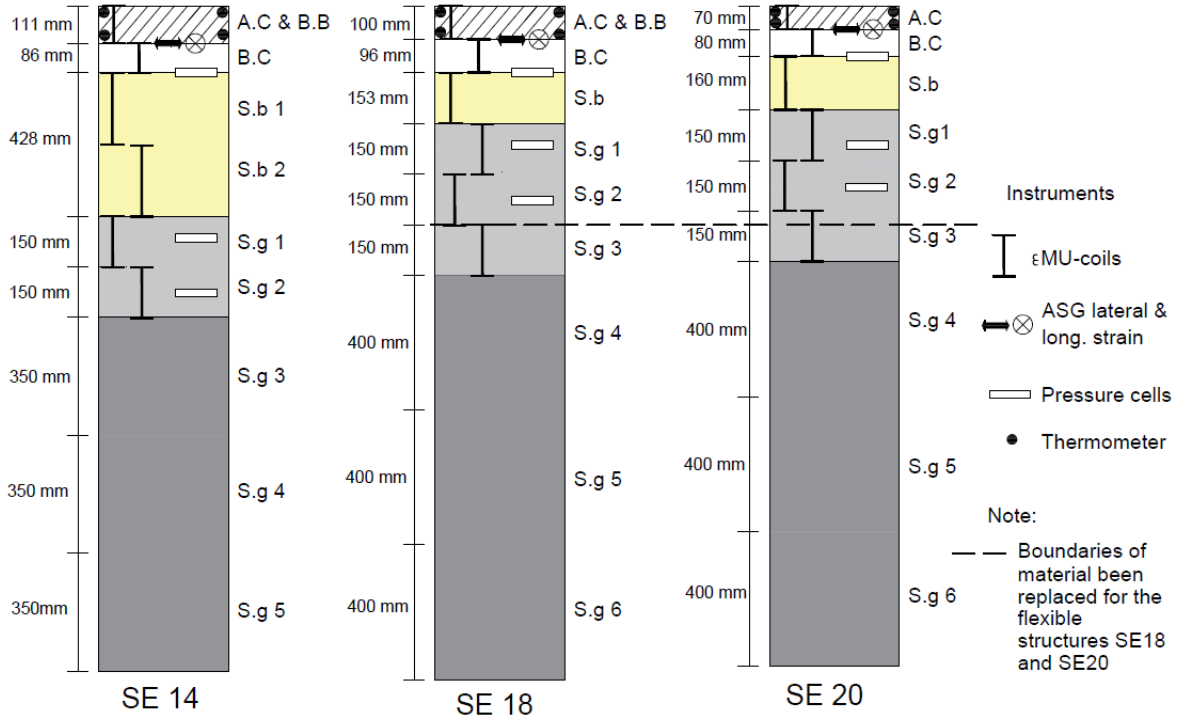

Figure 4.4 Cross section of structure SE14, SE18 & SE20 (Arvidsson, 2014). A.C means asphalt concrete, B.B means bituminous binder, B.C means base course, S.b means subbase and S.g means subgrade.

For structures SE18 and SE20, the material below 650mm depth was not replaced, as per Ardvisson, (2014).
A short description of the instrumentation follows below. For more detailed description see Saevarsdottir et al., (2015).

4.2.1 Soil pressure cell (SPC) type Geokon model 3500

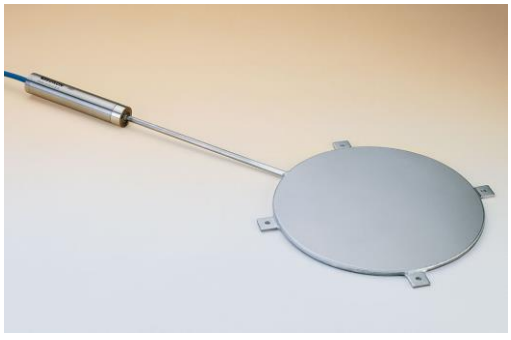

Figure 4.5 Geokon Model 3500.

The soil pressure cells Geokon model 3500 were used to measure stresses in base, subbase and subgrade layers (see Figure 4.5).

This cell consists of two stainless steel plates welded together at its border and separated by a small gap filled with hydraulic fluid. During loading the surrounding soil presses the two plates together creating an equal pressure in the internal fluid.

The accuracy of the measurements is specified as +/- 15% of the mean soil stress. The compaction and installation of the cells play an important factor in the results.

A total of three SPC where installed at the bottom of the base layer (figure 4.4), and another two at different elevations in the subgrade layer. Nottingham pressure cells were also used. They are made of a titanium disc that is a diaphragm attached rigidly to a guard ring. A four-arm-gouge bridge is attached to the diaphragm and connected to reduce sensitivity. This instrument is suitable for transient or short-term stress measurements (NTEC, 2013).

4.2.2 εMU coils

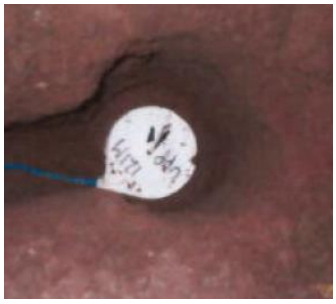

Figure 4.6 εMU coil.

A soil-strain measuring system (εMU) developed by the University of Nottingham was used to measure the displacement in the vertical direction (see Figure 4.6). As load is applied an alternating current is passed through one coil, generating an electromagnetic signal that is received by other plate. The current is proportional to the displacement. The dynamic (elastic) and permanent (plastic) strain can be measured by the system (Dawson, 1994). Three columns where installed in each of the trial pits, seven coils in each column for a total of twenty-one coils for each pavement structure.

4.2.3 H-shaped asphalt strain gauges from Dynatest (ASG)

Figure 4.7 H-bar strain.

Dynatest gauges (H-Bar shape) are used to measure the horizontal tensile strain at the bottom of the asphalt layer (see Figure 4.7). A good bond between the gauge and the surrounding material will provide strain values close to theoretical estimation (Dynatest, 2014).

A total number of eight ASG where installed in each structure in the interphase between the asphalt and the base layer.

4.2.4 Laser for surface rut measurement

Laser beams were used to measure the pavement profile (rut) on all structures. Laser measurements are used specifically to measure the surface rut of the asphalt structure and are fundamental information for the calculation of the PD.

4.3 Behavior of the pavement structure

One of the objectives of this thesis is to find the main material parameters for the structures SE14, SE18 and SE20 with backcalculation. Using data from FWD for backcalculation can provide enough tools to arrive at accurate material parameters when all deformation, stress, and strain curves are compared. The best fit parameter combinations should also match all

the measured data of the three flexible structures, this means, FWD deflection curve, stress, strain, and tensile strain must match to each other. An extensive number of graphs with different parameter combinations were compared to get the best fit values with the minimal error. Standard deviation on FWD graphs is used to determine if the measurements fit the model parameters.

A vast amount of raw data for the FWD and HVS tests for SE14, SE18 and SE20 was received from VTI. Additionally, particle size distribution curves, plate load test, and other general material parameters of the layers of the three structures are available from VTI report 35-2014 (Arvidsson, 2014).

On the other hand, before starting the backcalculation, no data was available for the Young and resilient modulus of any of the layers or k_1, k_2 or k_3 coefficient values. For this work, repeated-load triaxial test (RLT) was not available to estimate the nonlinear coefficients of the unbound materials. It is well known that RLT test are time consuming and expensive.

4.3.1 Backcalculation of material properties

The initial material properties where based on previously obtained results from similar testing.

From FWD test measurements and the comparisons with ERAPAVE results, the main parameters of the structures are summarized in Tables 4.3, 4.4 and 4.5.

All structures were analysed at different load conditions from very light to heavy and with different tire pressures. Dual wheel loading was mainly used for the analysis and comparisons.

In general, good agreements were found between the calculations and the measured surface deflection.

The best fit k_1 value found for the base course layer was 500 for SE14 and SE18 with k_2 equal to 0.6. This value is the same found by Saevarsdottir, (2014). For SE20 the best fit value for k_1 in the base course layer was 250 with k_2 equal to 0.6. For SE20 the different k_1 value can be explained when comparing the different modulus of deformation (E_{v2}) values for SE20 to SE14 (Arvidsson, 2014). The E_{v2} for SE14 base course was 156 ± 12 [MPa/m^2] and for SE20 this value was 74.0 ± 3.0 [MPa/m^2].

The difference in the asphalt Young´s modulus of the three asphalt layers for the FWD test is due to the temperature dependency of the layer when performing the nondestructive test. The FWD for SE14 & SE20 was performed at 13^{o}C and for SE18 the temperature was 4^{o}C. Equation (5) was used to get E_{ref} = 6000 MPa at 10^{o}C as a common value of E for the three asphalt layers. On the other hand, the temperature for the HVS test was always set at 10˚C.

The subbase course of Structure SE14, was divided into two sublayers. It was noticed on the vertical strain graphs that there was a big difference in the measurements between these two subbase layers, and the backcalculation shows a factor value of 2 between them. The reason for this is probably different compaction during construction stages, but this information has not been reported or mentioned in any document. It is also expected that

the lower layers are more compacted than the upper layers, which is normal due to the construction sequencing of the structure.

Only a portion of the subgrade material for the structures SE18 and SE20 was replaced when the structures were built, and it was noticed that in the vertical strain graphs there is a small difference on the two different subgrade layers. This difference between the old and new sand subgrade was modelled dividing the subgrade layer into two different layers. It is expected more compaction on the old layer with the same material.

Table 4.3 Resume of material parameters for pavement structure SE14.

Layer	Thickness	Falling Weight Deflectometer Young / Resilient Modulus			Heavy Vehicle Simulator Stiffness / Resilient Modulus			Unit weight
	h [mm]	E [MPa]	k_1 [-]	k_2 [-]	E [MPa]	k_1 [-]	k_2 [-]	γ [kN/m³]
A.C	32	5000	-	-	3500	-	-	25.27
B.B	79	5000	-	-	3500	-	-	25.91
B.C	86	-	500	0.6	-	500	0.6	22.1
S.b 1	214	-	1200	0.6	-	1200	0.6	22.1
S.b 2	214	-	2400	0.6	-	2400	0.6	22.1
S.g	-	160	-	-	60	-	-	18.2

Poisson´s ratio ν [-] = 0.35; k_o = 0.6 Typical for all layers
k_3 [-] = 0; Typical for course materials

Table 4.4 Resume of material parameters for pavement structure SE18.

Layer	Thickness	Falling Weight Deflectometer Young / Resilient Modulus			Heavy Vehicle Simulator Stiffness / Resilient Modulus			Unit weight
	h [mm]	E [MPa]	k_1 [-]	k_2 [-]	E [MPa]	k_1 [-]	k_2 [-]	γ [kN/m³]
A.C	47	7700	-	-	3500	-	-	25.27
B.B	53	7700	-	-	3500	-	-	25.91
B.C	96	-	500	0.6	-	500	0.6	23.5
S.b	153	-	1200	0.6	-	1200	0.6	22.5
S.g 1 & 2	301	140	-	-	140	-	-	18.2
S.g	-	160	-	-	60	-	-	18.2

Poisson´s ratio ν [-] = 0.35; k_o = 0.6 Typical for all layers.
k_3 [-] = 0; Typical for course materials.

Table 4.5 Resume of material parameters for pavement structure SE20.

Layer	Thickness	Falling Weight Deflectometer Young / Resilient Modulus			Heavy Vehicle Simulator Stiffness / Resilient Modulus			Unit weight
	h [mm]	E [MPa]	k_1 [-]	k_2 [-]	E [MPa]	k_1 [-]	k_2 [-]	γ [kN/m³]
A.C	70	5000	-	-	3500	-	-	25.27
B.C	80	-	250	0.6	-	250	0.6	23.5
S.b	160	-	1200	0.6	-	1200	0.6	22.5
S.g 1 & 2	340	140	-	-	140	-	-	18.2
S.g	-	160	-	-	60	-	-	18.2

Poisson´s ratio v [-] = 0.35; k_o = 0.6 Typical for all layers.
k_3 [-] = 0; Typical for course materials.

Modifications on the values found on the FWD test for the E and M_r are required when using the data for the HVS test. The main reason is that the speed of loading for the test in the FWD is faster than the HVS (12 km/h) and this causes the E and M_r of the asphalt layer and subgrade to be higher in the FWD test (Saevarsdottir, 2014). The E and M_r are calculated for FWD as 80km/h and for the HVS test it must go down to 12 km/h. From equations (6) and (7) and the master curves for AG 22 (Ahmed, 2014), the Young's modulus for HVS is 3500 MPa. This represents a ratio FWD/HVS of 1.71. This value agrees with the findings by Saevarsdottir, (2014). The new M_r value for the subgrade must be backcalculated and it was found to be 60 MPa. The modification for the E and M_r is applicable to all the three flexible structures and for all the graphs where HVS data was used (vertical and horizontal strain, vertical stress).

4.3.2 Falling weight deflectometer (FWD)

Figures 4.8, 4.9 and 4.10 present the comparison between the measured and computed measurements for the FWD. For the three models, correlations were found for the heavy loading at 50 kN and 65 kN. Priority was given to get the best fit comparison for the load at 50 kN because it is the more normal single axle load expected during the life cycle of the asphalt structure in Sweden. Loads over 65 kN are very seldom or unexpected. Agreeability between the constants and parameters is also considered when the model over-predicts the surface deflection on the vicinity of the center of the plate.

The asphalt layer for structure SE20 is thinner than the other two. For thinly surfaced structures, granular layers are closer to the applied load and can reflect the results seen in the following figures. The over-estimation on the measurements found in structure SE20 (Figure 4.10) are probably because the FWD test was performed after the HVS and one can expect the unbound layers to be more compacted and deformed.

The FWD tests for SE14 and SE18 were performed before the main HVS test. For SE20 the FWD test was carried out after the HVS test (after the 745000 load repetitions).

The standard deviation is also plotted to have a better idea of the amount of data analysed.

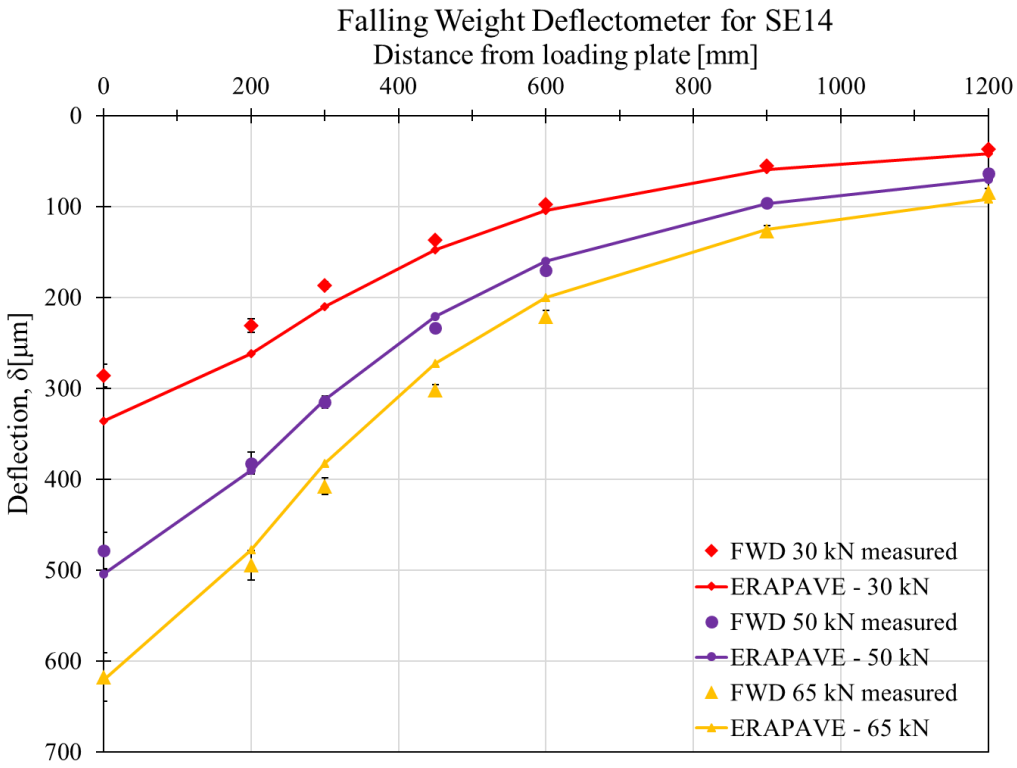

Figure 4.8 Falling Weight Deflectometer SE14.

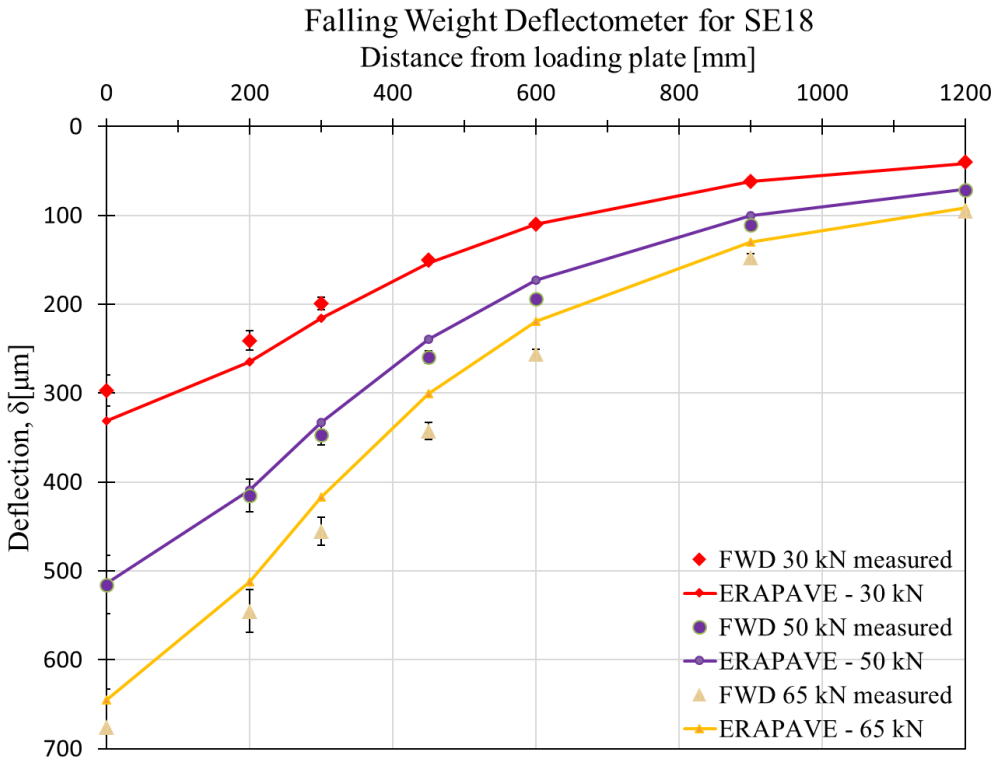

Figure 4.9 Falling Weight Deflectometer SE18.

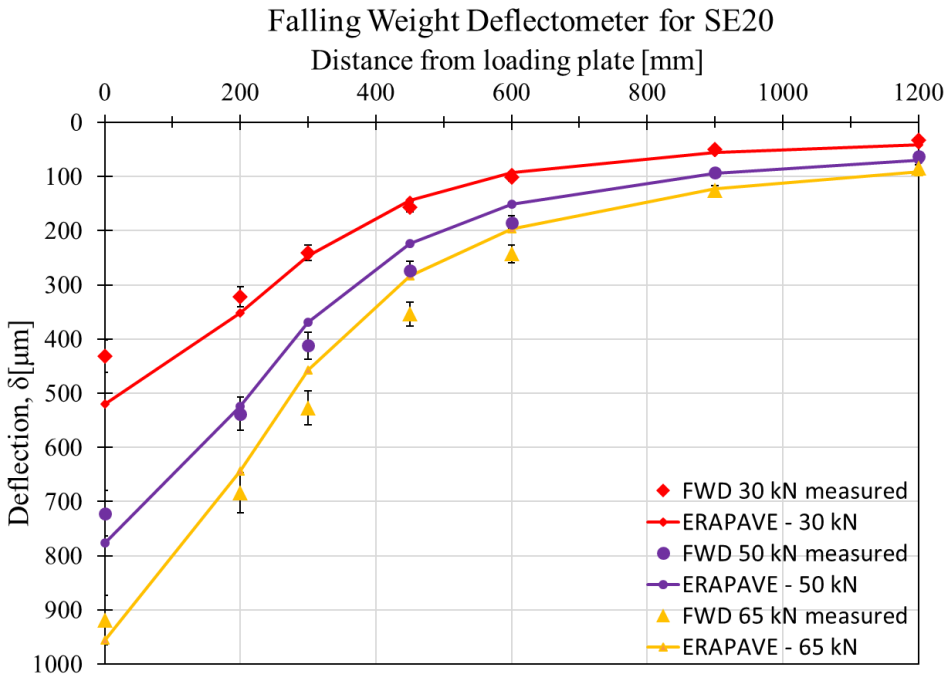

Figure 4.10 Falling Weight Deflectometer SE20 with measurements done after HVS test performed.

4.3.3 Vertical strain

Figures 4.11, 4.12 and 4.13 show the vertical strain measured and calculated at different load conditions, during the response phase, from very light to heavy load conditions (40 kN, 50 kN, 60 kN and 80 kN of half-axle load) with three different tire pressures 500 kPa, 800 kPa and 900 kPa. Dual wheel load configuration was considered in all the graphs.

As shown in Figure 4.4 the εMU sensors where installed over various depths at different locations, starting at the asphalt surface and ending at approximately 80-90 cm.

For SE14 and SE18, the average value of all the measurements was used. In general, good agreement was found between these two structures.

For structure SE20 the response measurements were carried out after 165000 load repetitions (unfortunately no response data were available after 20000 load repetitions as per structures SE14 and SE18). An over-estimation on the measured values can be seen for the heavy loading condition as shown in Figure 4.13 for dual wheel configuration (D.W) 80kN/800kPa. Additionally, not all the measured data was used for SE20 because some errors were found on the instrument's values.

The strain graphs are very relevant and used directly for the backcalculation of the material parameters. The stress and tensile strain graphs are also taken into consideration, but only to corroborate the agreement between all the material parameter been backcalculated.

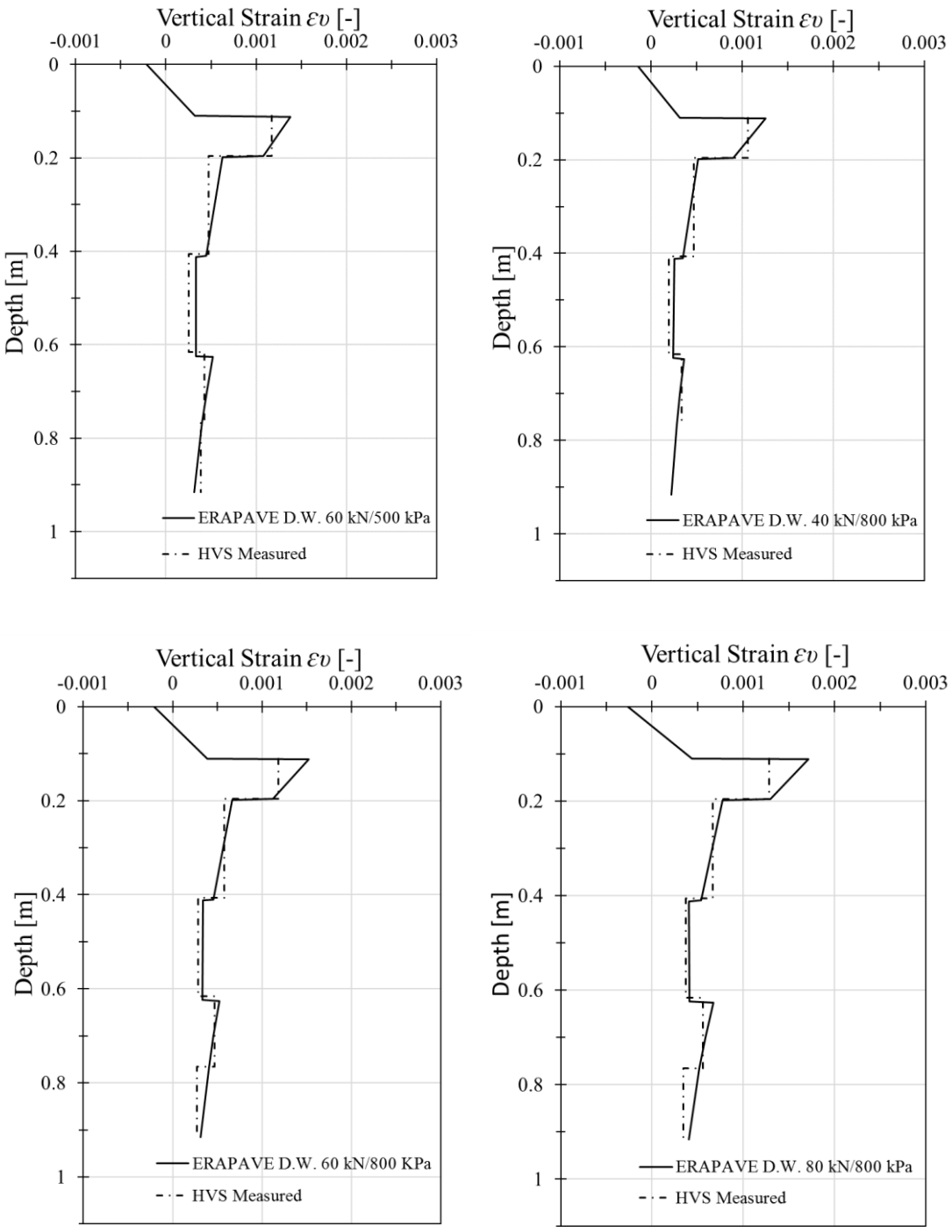

Figure 4.11 Vertical resilient strain as a function of depth for SE14 with different loads and tire pressure where D.W 40kN / 800kPa, means dual wheel configuration with 40kN on half-axle load with a tire pressure of 800kPa.

The response for structure SE14 was measurements after 20000 load repetitions.

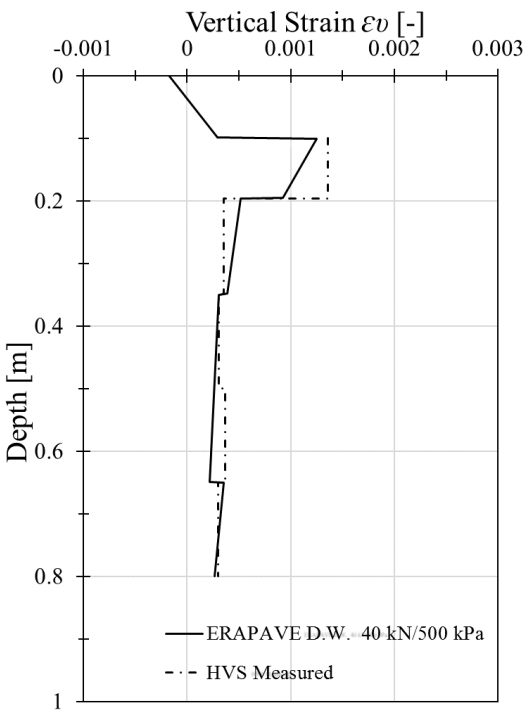
Vertical Strain εv [-]
-0.001
0
0.001
0.002
0.003
0
0.2
0.4
0.6
0.8
1
Depth [m]
ERAPAVE D.W. 40 kN/500 kPa
HVS Measured

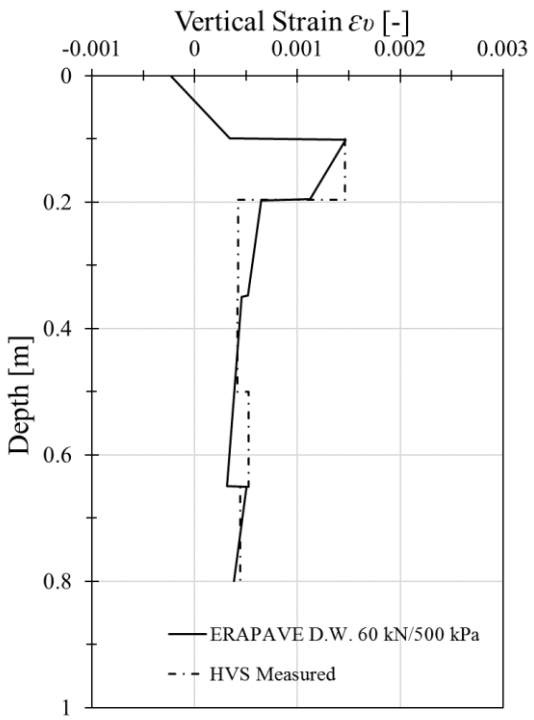
Vertical Strain εv [-]
-0.001
0
0.001
0.002
0.003
0
0.2
0.4
0.6
0.8
1
Depth [m]
ERAPAVE D.W. 60 kN/500 kPa
HVS Measured

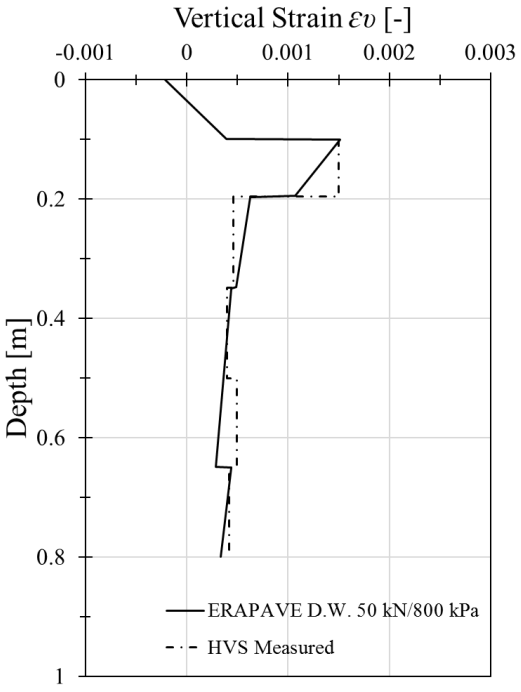
Vertical Strain εv [-]
-0.001
0
0.001
0.002
0.003
0
0.2
0.4
0.6
0.8
1
Depth [m]
ERAPAVE D.W. 50 kN/800 kPa
HVS Measured

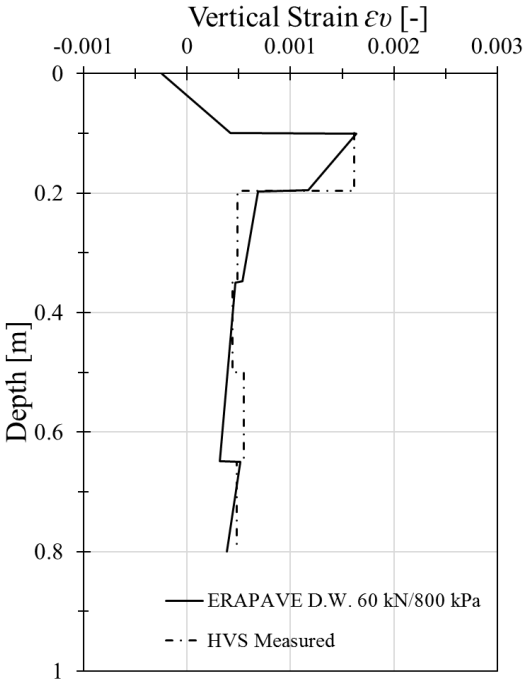
Vertical Strain εv [-]
-0.001
0
0.001
0.002
0.003
0
0.2
0.4
0.6
0.8
1
Depth [m]
ERAPAVE D.W. 60 kN/800 kPa
HVS Measured

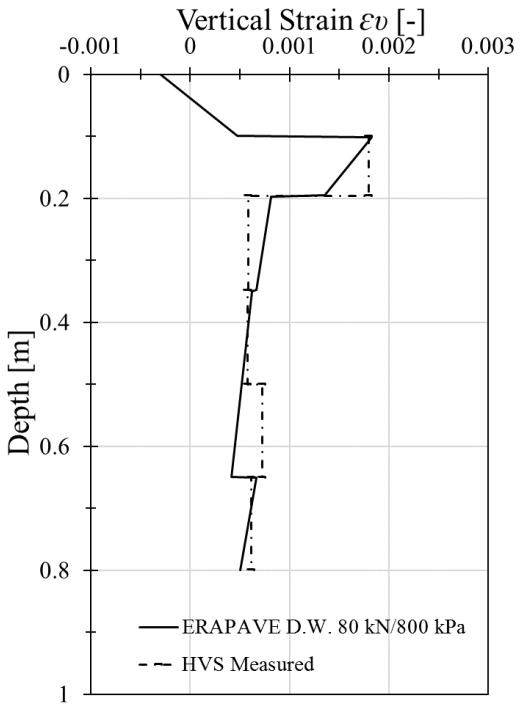

Figure 4.12 Vertical resilient strain as a function of depth for SE18 with different loads and tire pressure.

The response for structure SE18 was measurements after 20000 load repetitions.

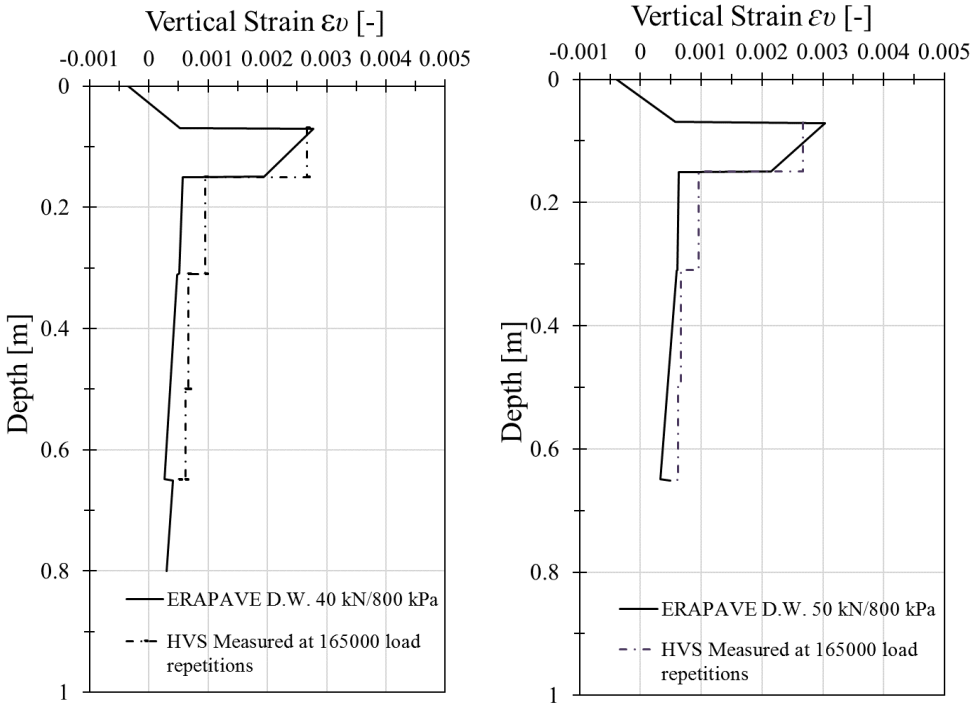

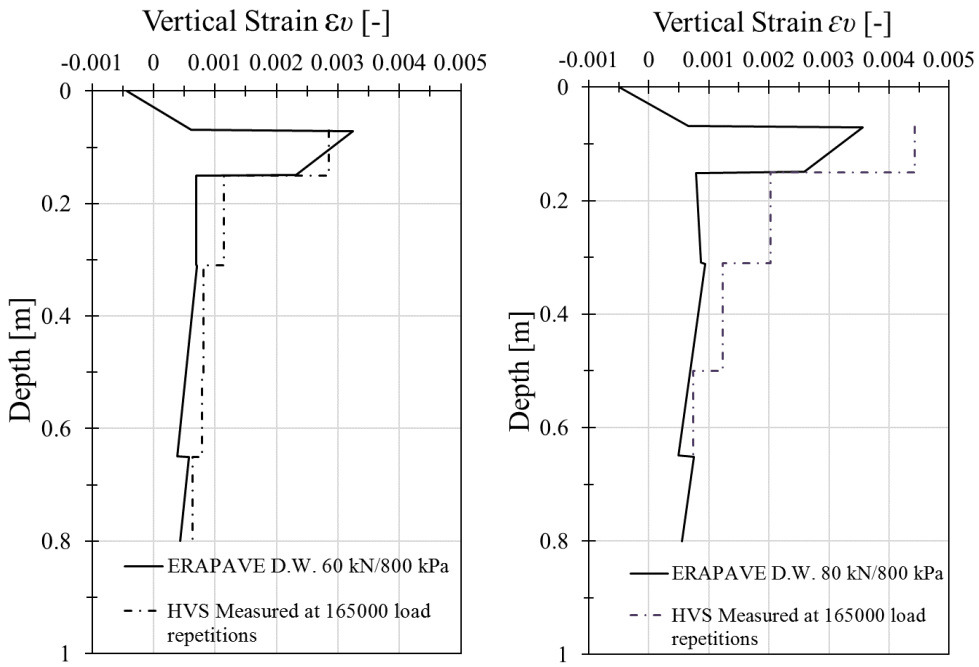

Figure 4.13 Vertical resilient strain as a function of depth for SE20 with different loads and tire pressure with measurements done after 165000 load repetitions.

The response for structure SE20 was measurements after 165000 load repetitions.

4.3.4 Vertical stress

Figures 4.14, 4.15 and 4.16 show the vertical stress analysed at different load conditions from very light to heavy load conditions (40 kN, 50 kN, 60 kN and 80 kN of half-axle load) with three different tire pressures 500 kPa, 800 kPa and 900 kPa. Dual wheel configuration was considered in all the graphs. For the three flexible structures, all the measured response data was used.

Good agreement between calculation and measurements was found for structure SE14 (see Figure 4.14). The response for structure SE14 was measurements after 20000 load repetitions.

For flexible structure SE18, as shown in Figure 4.14 good agreement was found between the measurements and calculations located at lower levels, and approximately 20% to 30% difference on the instrument located at 20 cm. Good measurements of vertical stresses are difficult to achieve in course base materials, and as specified by manufacturer, the accuracy of the instrument changes around ± 15% in some cases. The response for structure SE18 was measurements after 23000 load repetitions.

For SE20 the main inconvenience is to have response data only after 165000 load repetitions. An over-estimation on the measured values can be seen in Figure 4.16, including the values at lower levels.

As mentioned previously, the main emphasis for the backcalculation of the material parameters is put into the strain graphs.

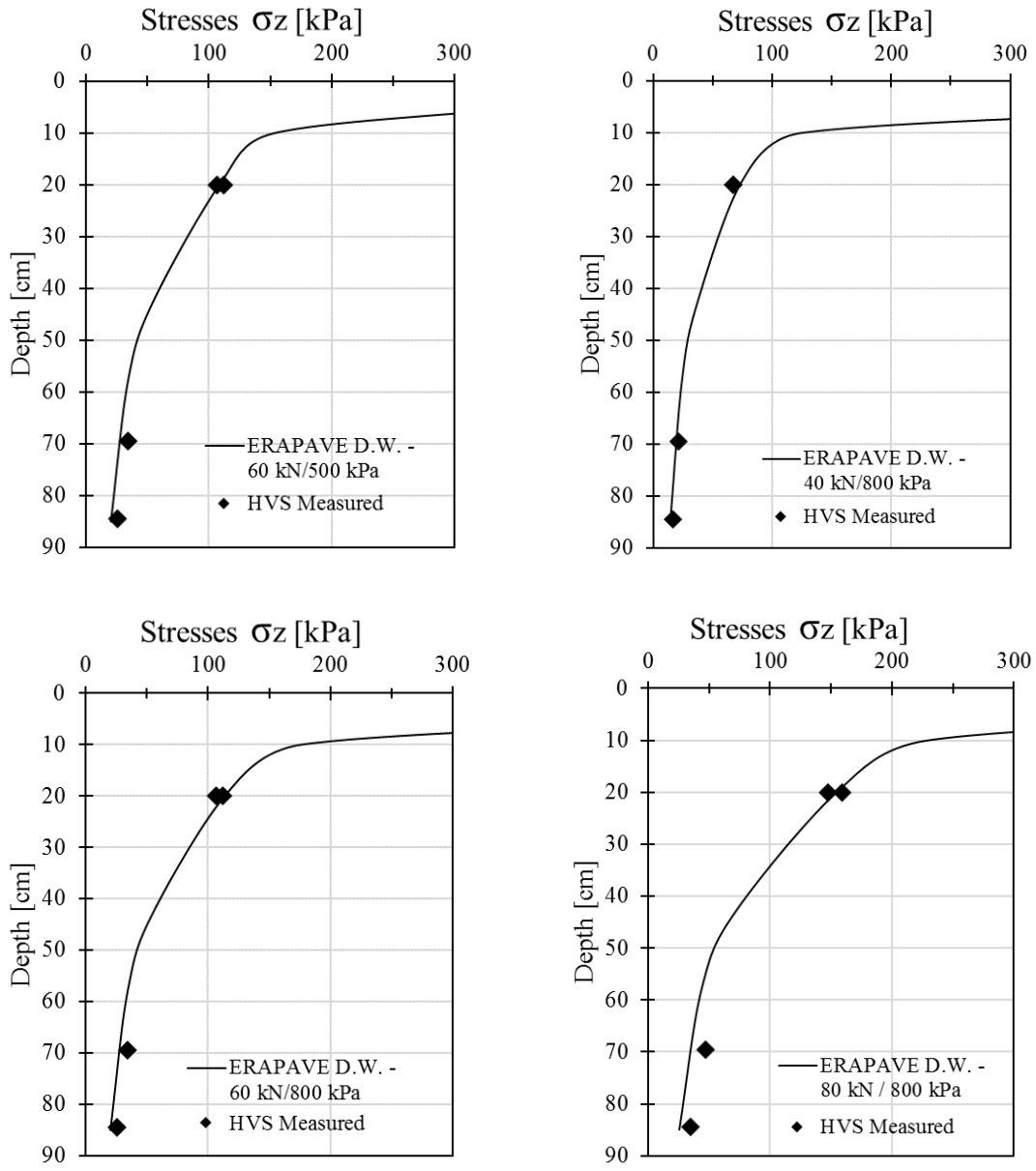

Figure 4.14 Vertical stress as a function of depth for SE14 with different loads and tire pressure where D.W. 40kN / 800kPa, means dual wheel configuration with 40kN on half-axle load and a tire pressure of 800kPa.

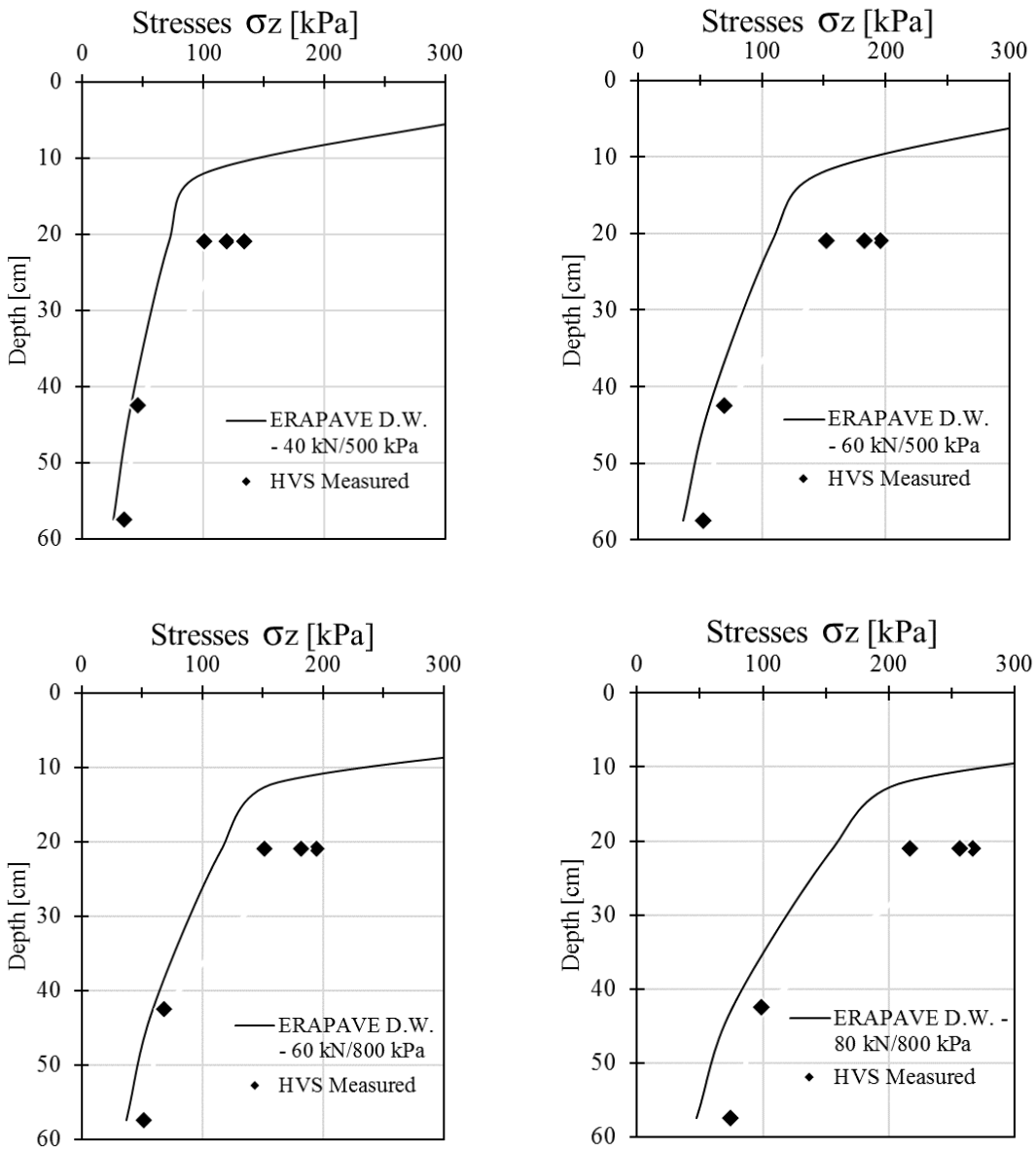

Figure 4.15 Vertical stress as a function of depth for SE18 with different loads and tire pressure.

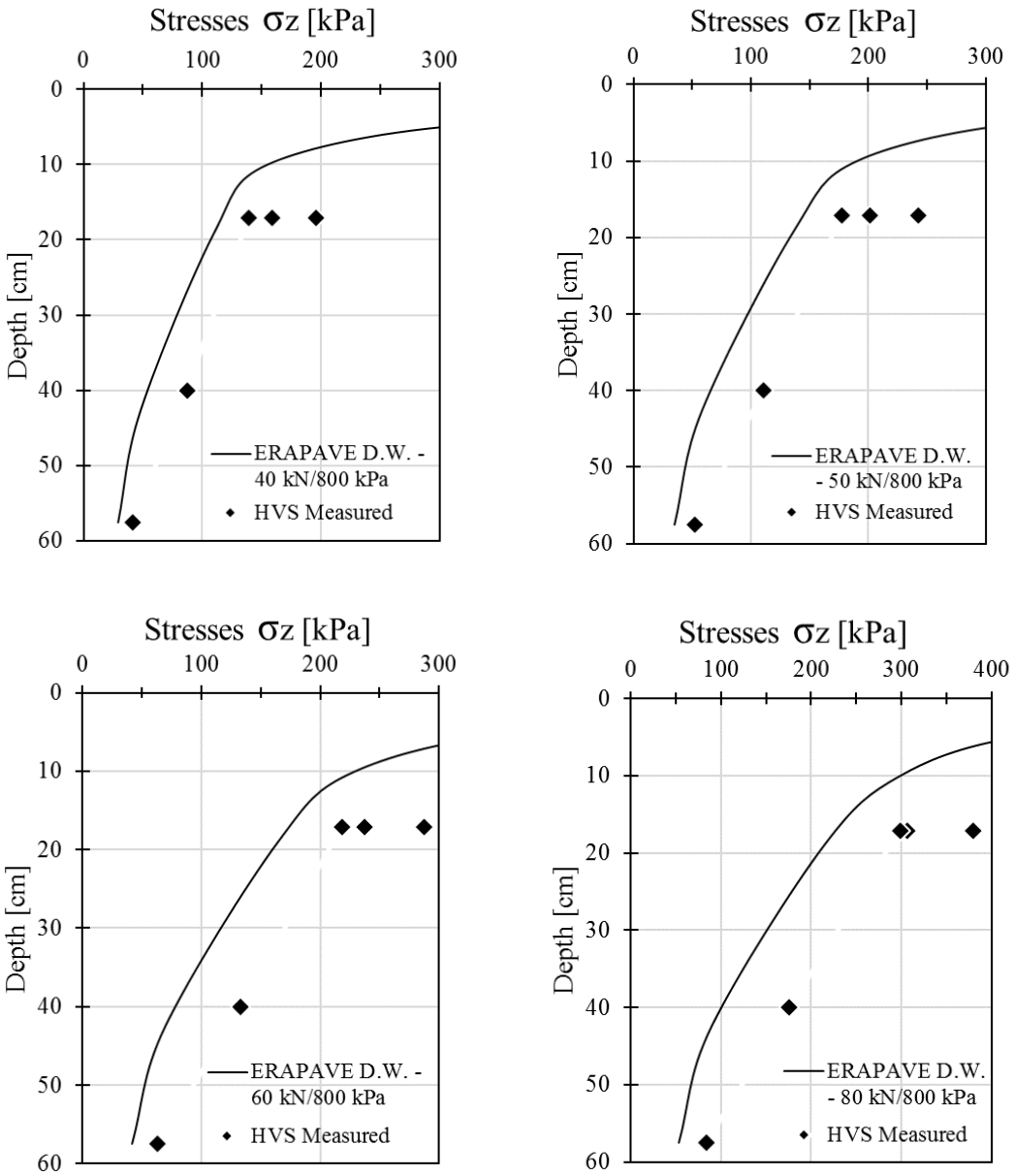

Figure 4.16 Vertical stress as a function of depth for SE20 with different load and tire pressures with measurements done after 165000 load repetitions.

4.3.5 Horizontal strain

The graphs on Figure 4.17 show the comparison of measured and computed horizontal strain for different load conditions from very light to heavy load. The load conditions used on the figure below are:

S93 is load condition with single wheel with 40kN/800kPa half-axle load.

P93 is load condition with double wheel with 40kN/800kPa half-axle load.

S11 is load condition with single wheel with 80kN/800kPa half-axle load.

P11 is load condition with double wheel with 80kN/800kPa half-axle load.

S90 is load condition with single wheel with 60kN/500kPa half-axle load.

P90 is load condition with double wheel with 60kN/500kPa half-axle load.

The two strain instruments located at the corners of the pit were neglected due to noice in the signal.

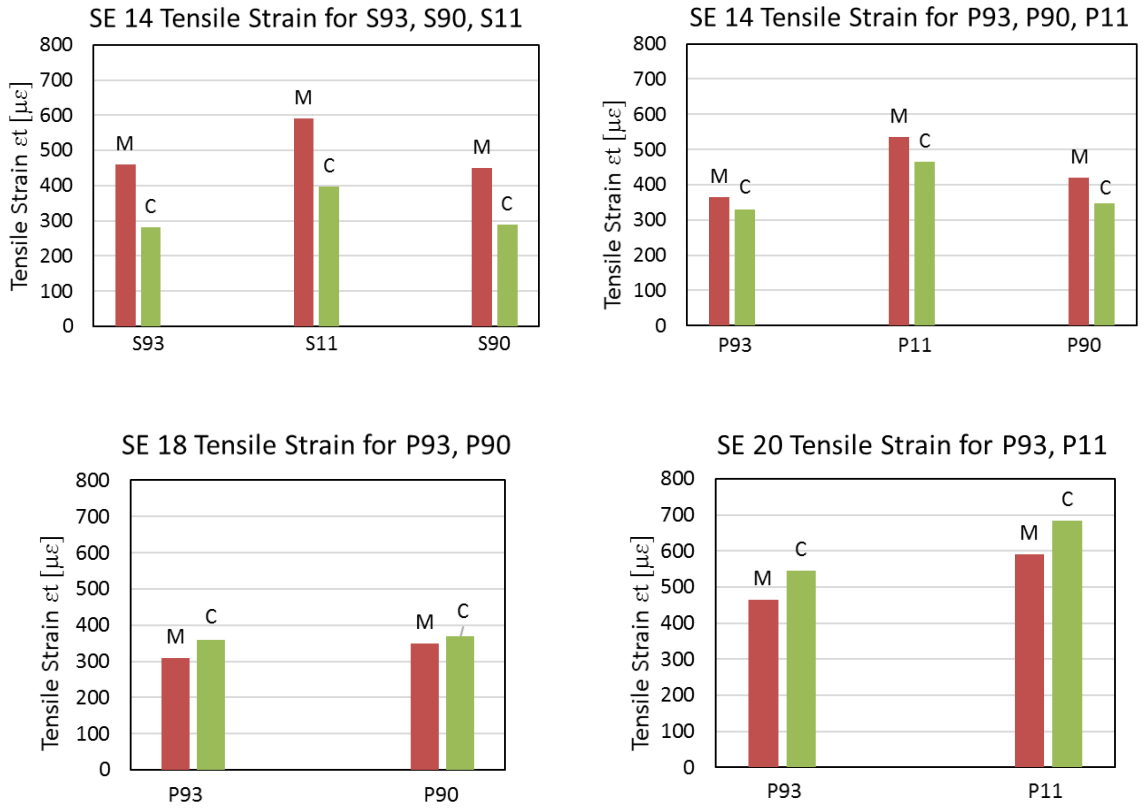

Figure 4.17 Comparison of measurements (M) and calculations (C) for horizontal strain for SE14, SE18 & SE20.

Only single wheel measurements for structure SE14 were available. In accordance to Figure 4.17, dual wheel loading gives better agreement than single wheels loading. It is difficult to generate conclusions on the reasons of why this happens and one of the possible explanation is due to the difference between the circular contact area assumed for the calculation with ERAPAVE and the most real rectangular shape of the wheel configuration. A calculation with a FEM analysis would be required to validate this assumption.

4.4 Predicting models

In general, good agreement was found between the rut measurements and the model calculated. The parameters backcalculated for the three structures with the time hardening approach shows promising results when comparing measurements and calculation.

4.4.1 Permanent deformation on structure SE18

4.4.1.1 Asphalt layer model

Equation (12) was used for the PD of the asphalt layer. The parameters used for equation (12) are given in Table 4.6.

Table 4.6 Asphalt model parameters for pavement structure SE18.

a_1 [-]	a_2 [-]	a_3 [-]	β_1 [-]
0.021	1.85	0.27	1.0

The asphalt mix layer for structure SE18 is composed of ABT 16 and AG 22. For AG22, a_1 = 0.0157 (Ahmed et al., 2014a). For ABT16 the assumed value is a_1 = 0.0249. The average value of the HMA mix is a_1 = 0.021.

The total asphalt layer thickness for SE18 is 10 cm. For the calculation, the layer was divided into two sublayers, and the analysis was performed on the middle of each sublayer, this means at 2.5 cm and 7.5 cm depth. The values for the vertical elastic strain (ε_r) at 2.5 cm at different lateral wander distribution (0 cm, 5 cm, 10 cm, 15 cm, 20 cm and 25 cm) shows negative values due to the tension generated by the wheel at the proximity of the surface to the layer. To be able to use equation (14), when ε_r was negative, it was changed to its absolute value only for the calculation of the N_{eq1}. For the final value calculated for $\Delta\varepsilon_p$ the original negative and positives signs were kept.

The two final strain values (ε_p) at 2.5 cm and at 7.5 cm where summoned to get the final predicted permanent strain of the total layer.

Figure 4.18 shows good agreement when comparing the site measurement and the computational values using ERAPAVE.

D.W 40kN / 800kPa stands for dual wheel configuration with 40kN on half-axle load with a tire pressure of 800kPa.

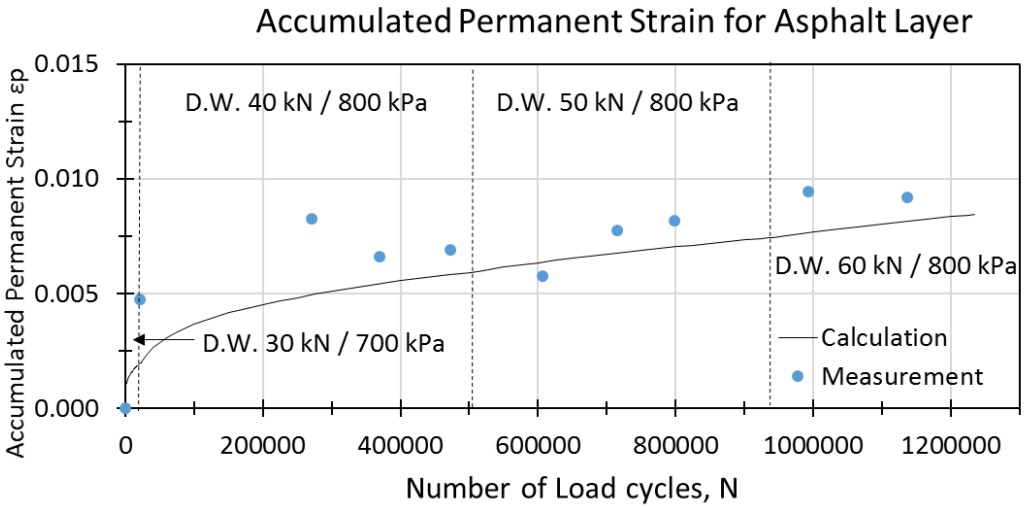

Figure 4.18 Predicted model for asphalt layer, structure SE18.

4.4.1.2 The unbound layer's model for SE18

Equation (10) was used for the prediction of the unbound layer. The value of *b* was kept constant for all the structure.

The *a* value was backcalculated and the values with best agreements are given in Table 4.7. Subgrade layer 3 is the last layer with instruments. From subgrade layer 4 all the *a* values are assumed to be half of the previous subgrade; this is mainly because more compaction on the lower layers of the structure is expected. Additionally, as shown in Figure 4.4, from subgrade layer 4 all the subgrade material was not replaced from previous test pIT and this condition needs to be taken into consideration for the selection of the *a* value. The time hardening or step load changes on the structure are after load repetition 23300, 501000 and 935000 (see Table 3.2 and Arvidsson, 2014).

Table 4.7 Predicted model for unbound material SE18.

SE18	Thickness [cm]	*a* [-]	*b* [-]
Base	9.6	0.0012	0.12
Subbase	15.3	0.0004	0.12
Subgrade 1	15.0	0.00017	0.12
Subgrade 2	15.0	0.00034	0.12
Subgrade 3	15.0	0.00045	0.12
Subgrade 4	40.0	0.00022	0.12
Subgrade 5	40.0	0.00022	0.12
Subgrade 6	40.0	0.00022	0.12
Total Layer	189.9		

The value of α in equation (9) is equal to 0.75.

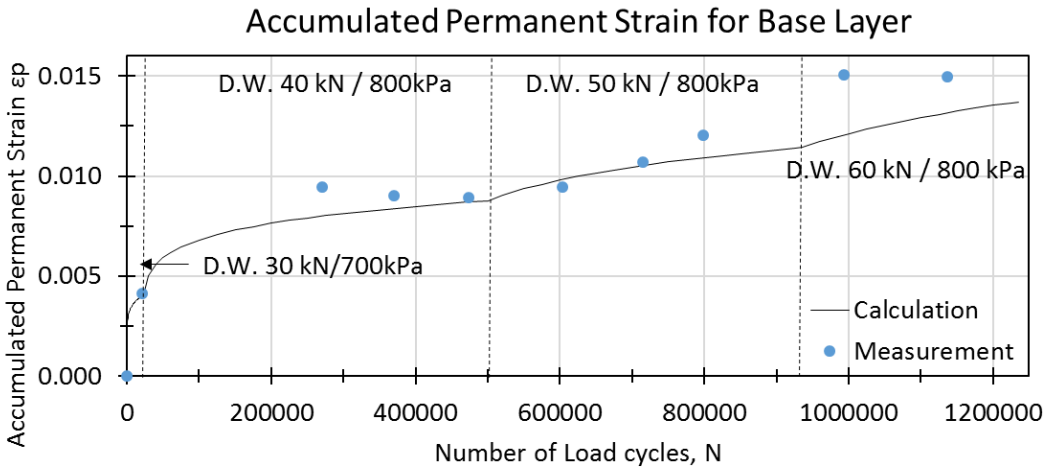

Figure 4.19 Accumulated permanent strain for base course layer, structure SE18.

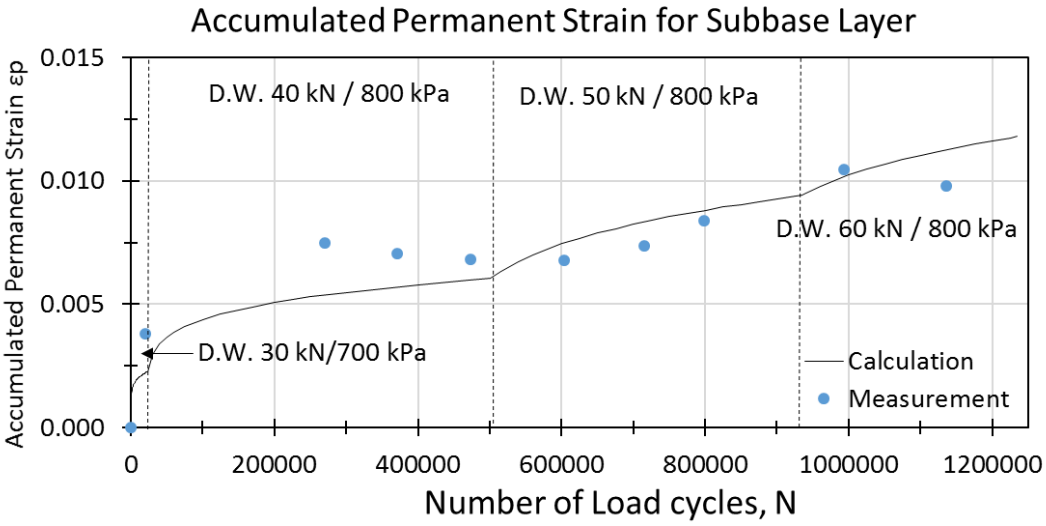

Figure 4.20 Accumulated permanent strain for subbase layer, structure SE18.

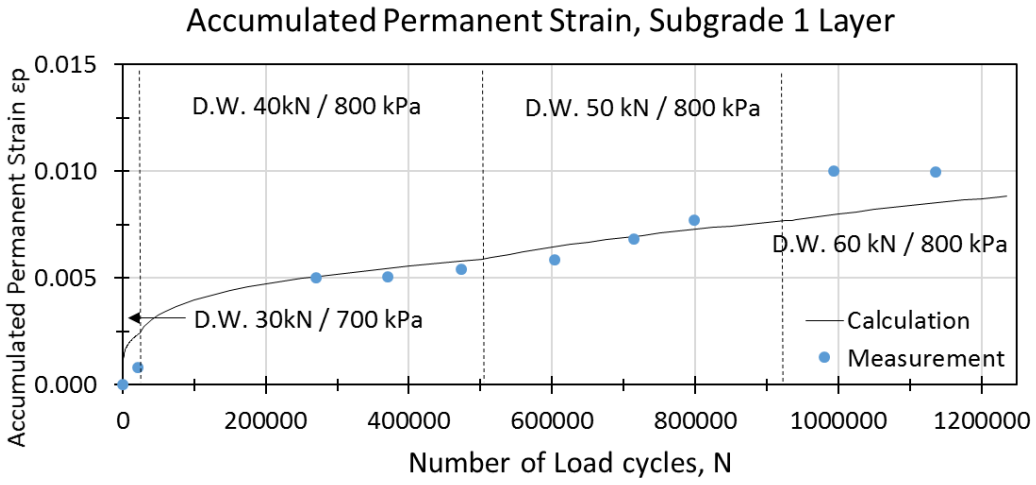

Figure 4.21 Accumulated permanent strain for subgrade 1 layer, structure SE18.

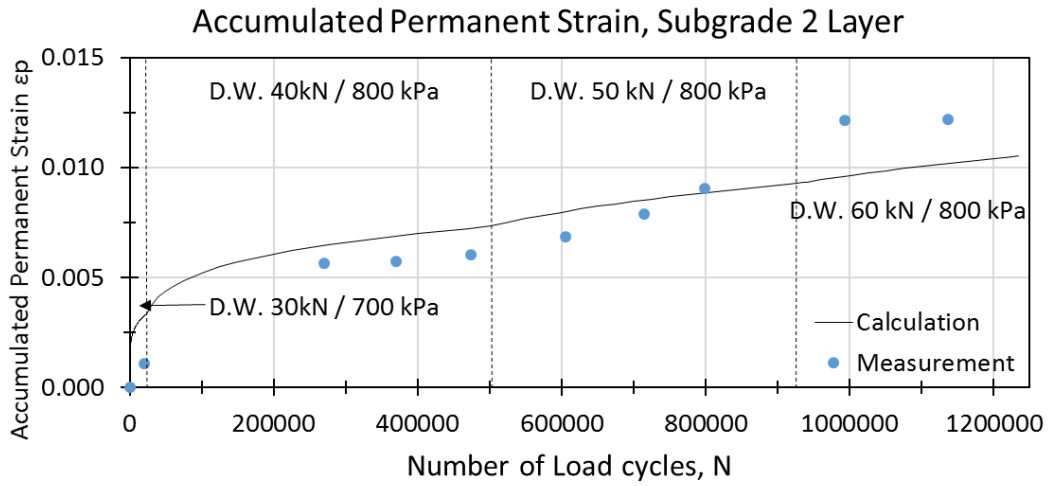

Figure 4.22 Accumulated permanent strain for subgrade 2 layer, structure SE18.

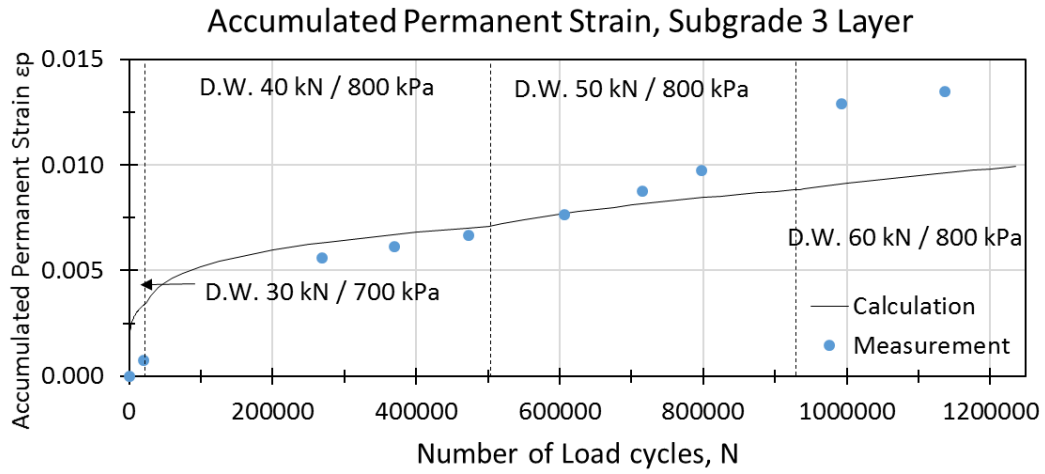

Figure 4.23 Accumulated permanent strain for subgrade 3 layer, structure SE18.

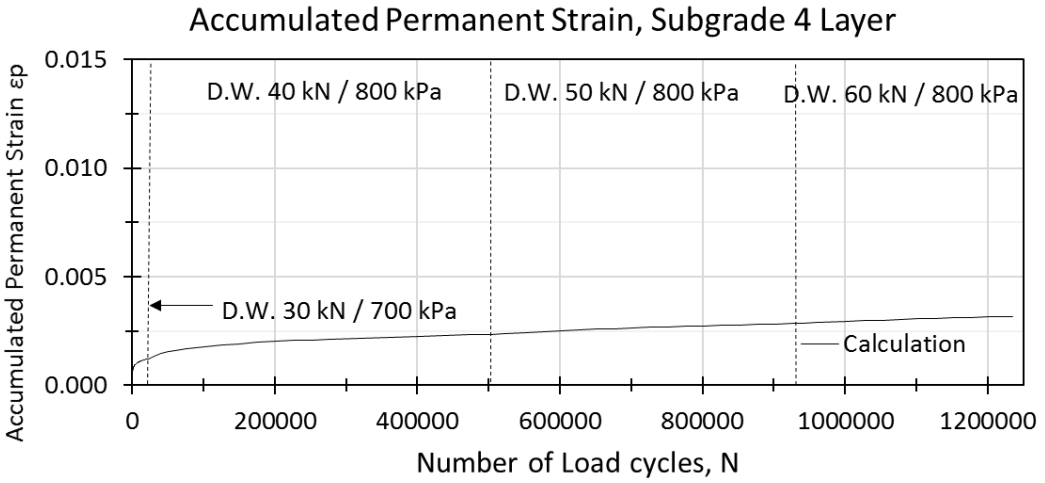

Figure 4.24 Accumulated permanent strain for subgrade 4 layer, structure SE18.

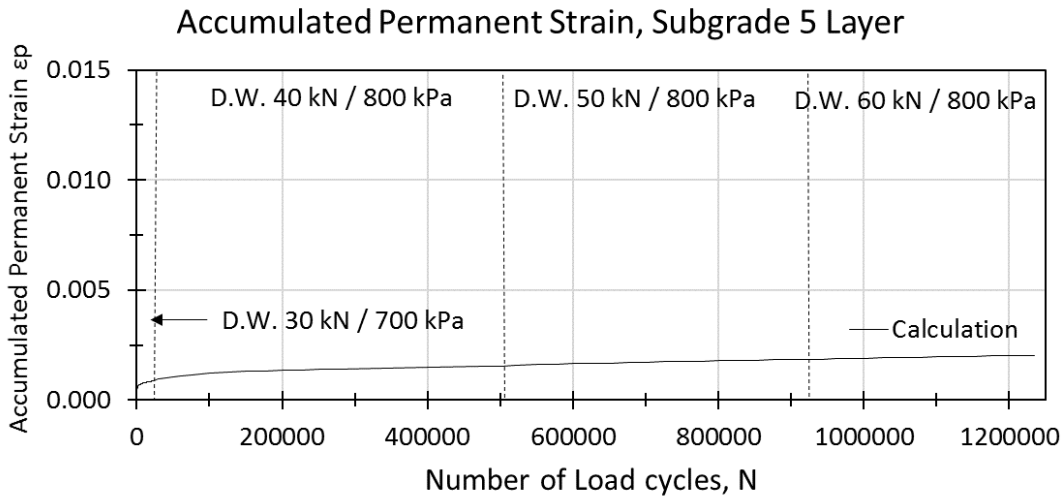

Figure 4.25 Accumulated permanent strain for subgrade 5 layer, structure SE18.

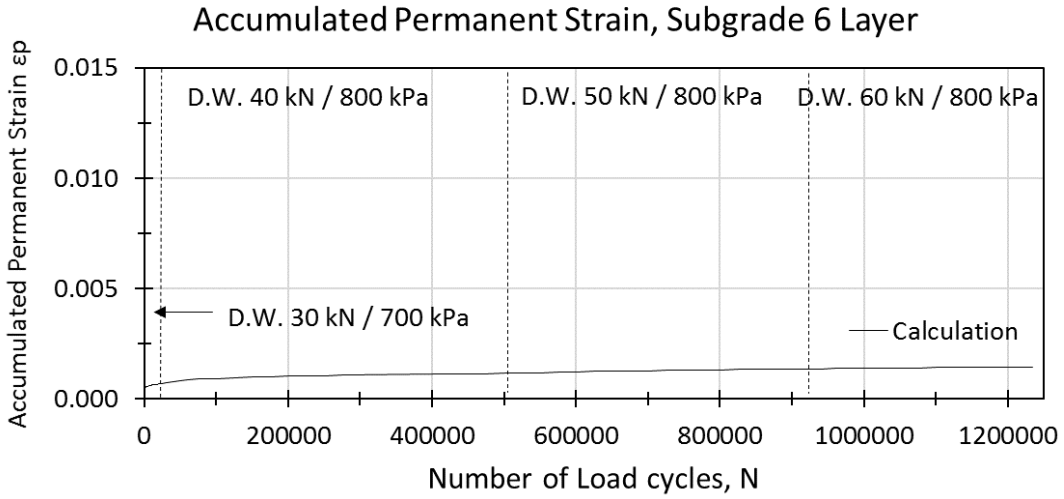

Figure 4.26 Accumulated permanent strain for subgrade 6 layer, structure SE18.

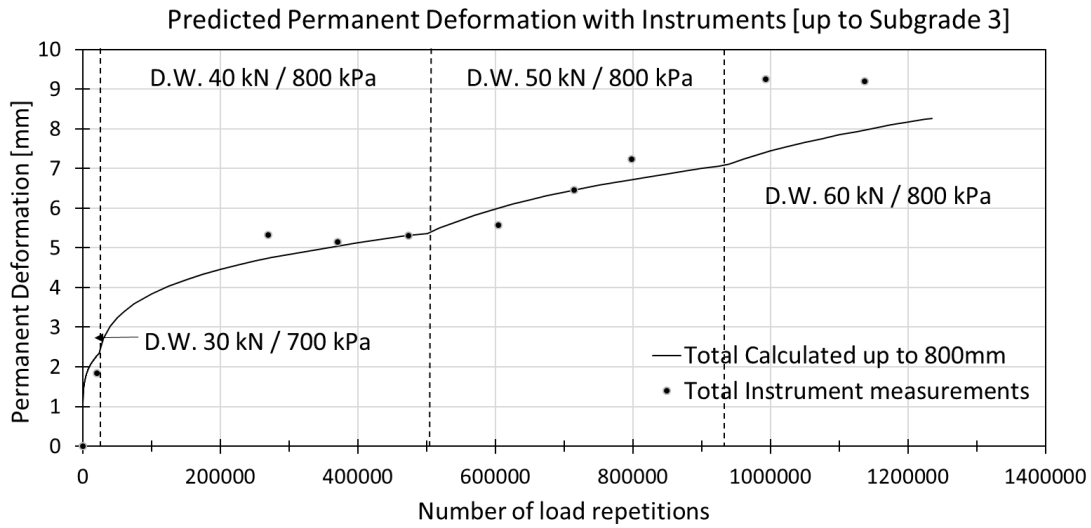

Figure 4.27 Predicted permanent deformation with instruments, structure SE18.

A good correlation is found for Figures 4.27 and 4.28, when comparing the measurements and the calculated prediction.

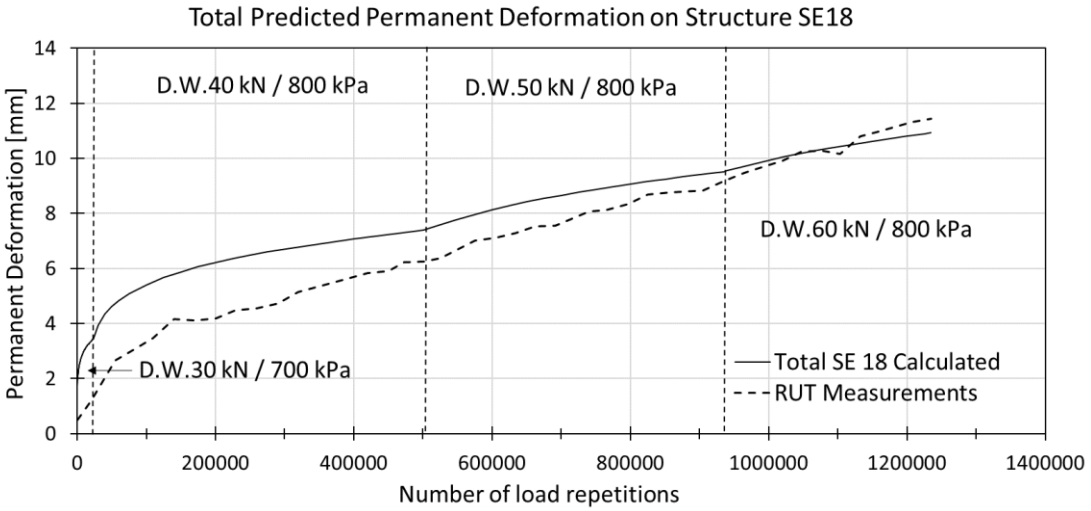

Figure 4.28 Total predicted permanent deformation on structure SE18.

For the SE18 structure of 199.9 cm, the total permanent deformation predicted at 1200000 load repetitions is 11 mm. The analysed model over-predicts the deformation values at the beginning of the load repetition, but provides good agreement at 1200000 load repetition. Unfortunately, only 2 measurements are available from 900000 load repetitions with applied load of 60kN/800kPa. More profile measurements are required to evaluate the overprediction on the permanent deformation at the last stage of the HVS test.

4.4.2 Permanent deformation on structure SE20

4.4.2.1 Asphalt layer

Equation (12) was used for the PD of the asphalt layer. The values used for equation (12) are given in Table 4.8.

Table 4.8 Asphalt model parameters for structure SE20.

a_1 [-]	a_2 [-]	a_3 [-]	β_1 [-]
0.0249	1.85	0.27	1.0

The asphalt layer for structure SE20 is ABT 16. Following the same assumption as SE18, a_1 = 0.0249.

The total asphalt layer thickness for SE20 is 7 cm. For the calculation, the layer was divided into two sublayers. This means the values used for the analysis at midpoint of each of the layers are at 1.75 cm and 5.25 cm respectively. Like structure SE18, the values in the proximity of the surface layer i.e. at 1.75 cm for the vertical elastic strain (ε_r) were negative for the lateral wander distribution (0 cm, 5 cm, 10 cm, 15 cm, 20 cm and 25 cm). To be able to use equation (14), when ε_r was negative, it was changed to its absolute value only for the calculation of the N_{eq1}. For the final value calculated for $\Delta\varepsilon_p$ the original negative and positives signs were kept.

The two final strain values (ε_p) at 1.75 cm and at 5.25 cm were summoned to get the final predicted permanent strain of the total layer.

Figure 4.29 shows good agreement when comparing the site measurement and the calculated values.

D.W 40kN / 800kPa stands for dual wheel configuration with 40kN on half-axle load with a tire pressure of 800kPa.

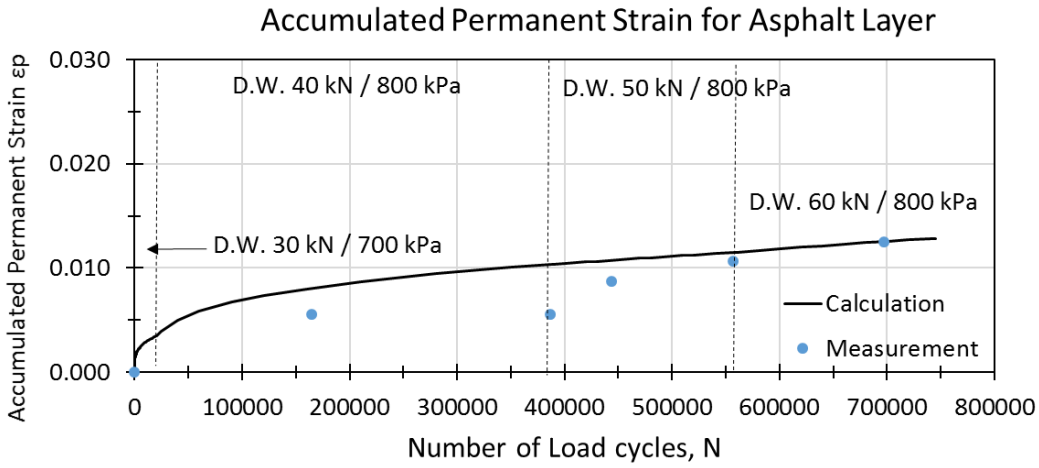

Figure 4.29 Predicted model for asphalt layer, structure SE20.

4.4.2.2 The unbound layer's model for SE20

Equation (10) was used for the prediction of the unbound layer. The value of *b* was kept constant for all the structures. The *b* value of 0.12 and 0.2 where compared with the site measurements, and the best agreement was found for $b = 0.2$. Based on laboratory tests on a similar model, the *b* value is highly dependent on the degree of compaction (Rahman et al., 2015). The only measurement available to compare the degree of compaction was on report by Arvidsson, (2014). This report shows that the base layer structure for SE20 is less compacted than SE18 when comparing the E_{v1} and E_{v2} values. Unfortunately, this is the only evidence to support the difference in *b* values between the structures SE18 and SE20.

The *a* value was backcalculated and the best agreements are given in Table 4.9. The *a* value is highly dependent of the moisture content, i.e. the higher the moisture content, the higher the *a* value, and also its compaction degree and grain size distribution (Rahman et al., 2015). Using Figure 19 and 26 from (Arvidsson, 2014), the moisture content is higher for structure SE18 than SE20, and this is in agreement with the higher values found for SE18 for the *a* value.

The value of α in equation 9 is equal to 0.75, similar to SE18.

Table 4.9 Predicted model for unbound material SE20.

SE20	Thickness [cm]	*a* [-]	*b* [-]
Base	8.0	0.0012	0.2
Subbase	16.0	0.00008	0.2
Subgrade 1	15.0	0.00006	0.2
Subgrade 2	15.0	0.00015	0.2
Subgrade 3	15.0	0.0002	0.2
Subgrade 4	40.0	0.0001	0.2
Subgrade 5	40.0	0.0001	0.2
Subgrade 6	40.0	0.0001	0.2
Total Layer	189.0		

Subgrade layer 3 is the last layer with instruments. From subgrade layer 4 all the *a* values are assumed to be half of the previous layer, this is mainly because more compaction is expected on the lower layers of the structure. Additionally, as shown in Figure 4.4, from subgrade layer 4 all the subgrade material was not replaced from previous test tip and this condition needs to be taken into consideration for the selection of the *a* value. The step load changes on the structure are after load repetition 20000, 387000 and 557000 (Arvidsson, 2014).

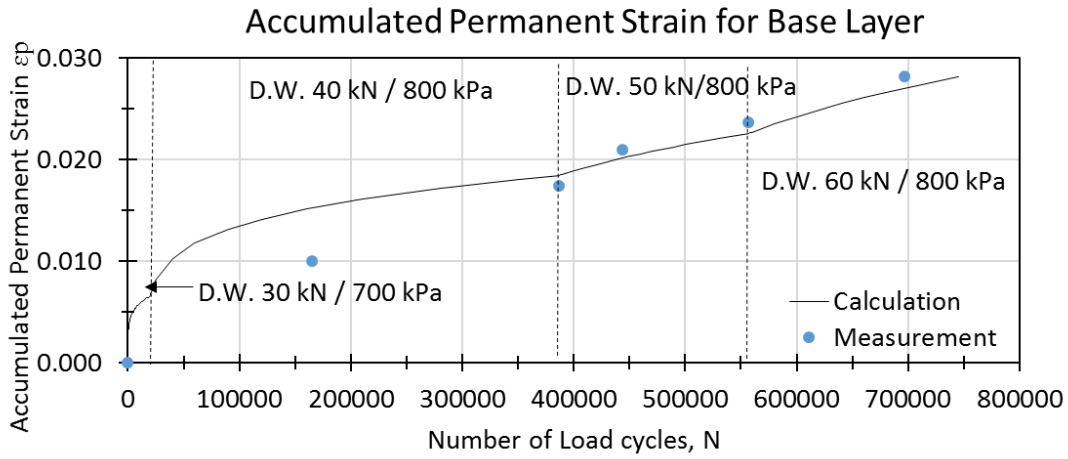

Figure 4.30 Accumulated permanent strain for base layer, structure SE20.

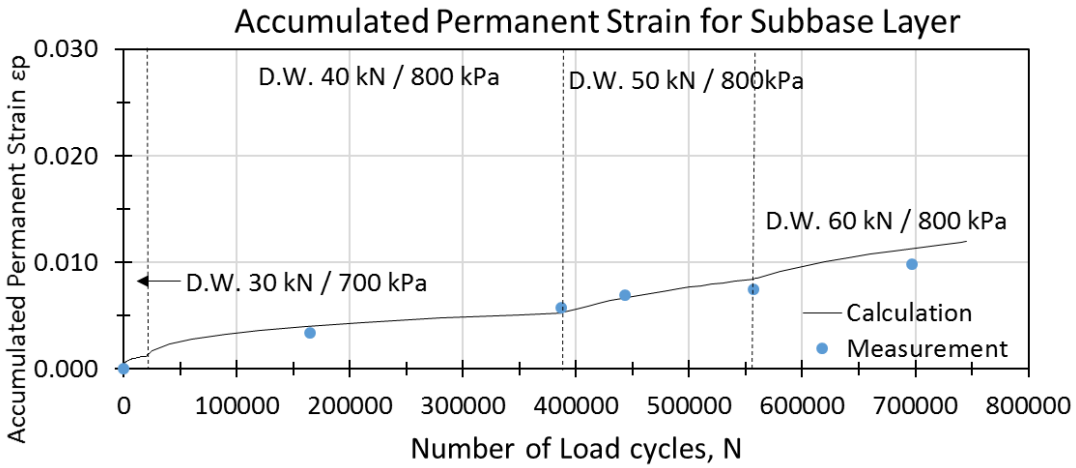

Figure 4.31 Accumulated permanent strain for subbase layer, structure SE20.

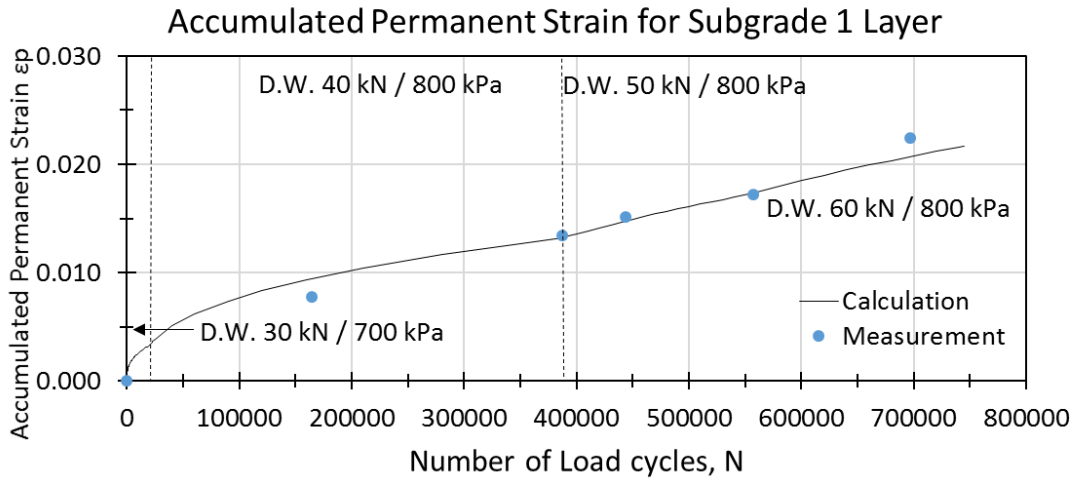

Figure 4.32 Accumulated permanent strain for subgrade 1 layer, structure SE20.

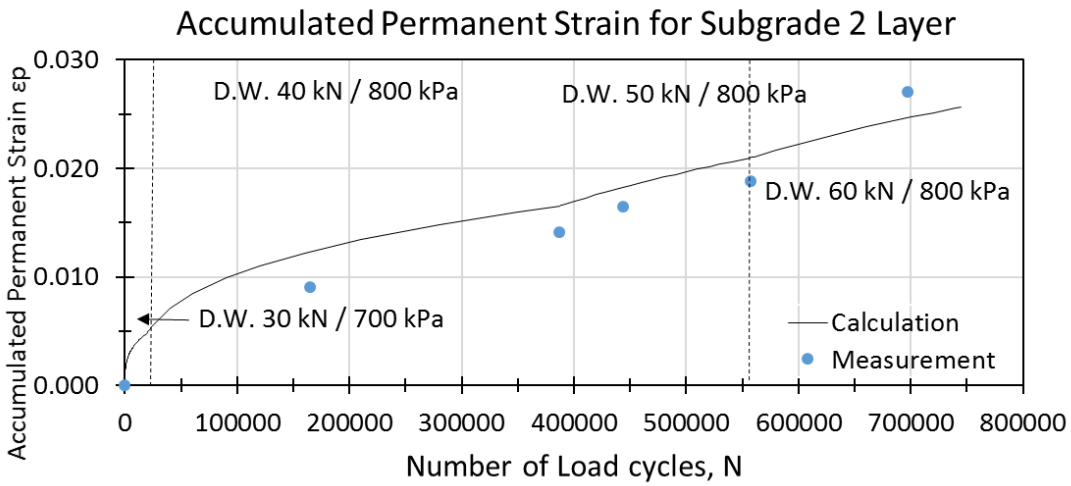

Figure 4.33 Accumulated permanent strain for subgrade 2 layer, structure SE20.

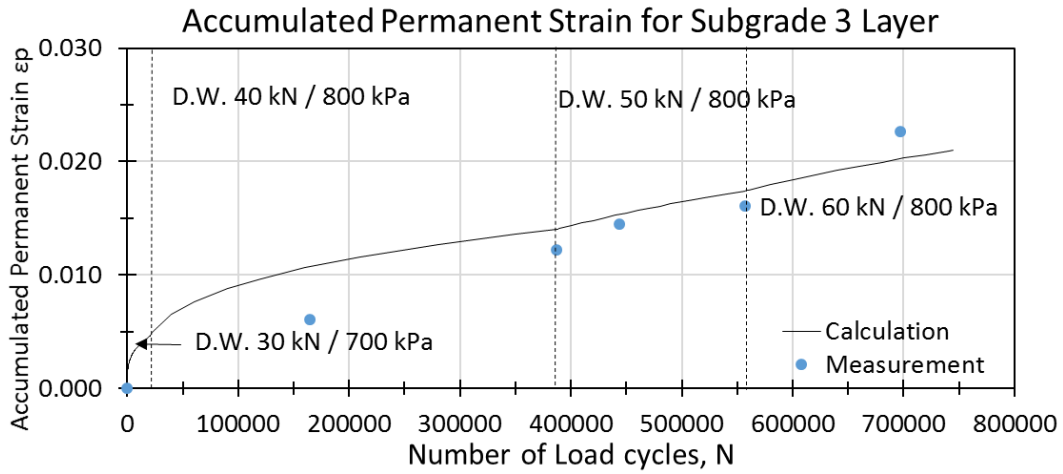

Figure 4.34 Accumulated permanent strain for subgrade 3 layer, structure SE20.

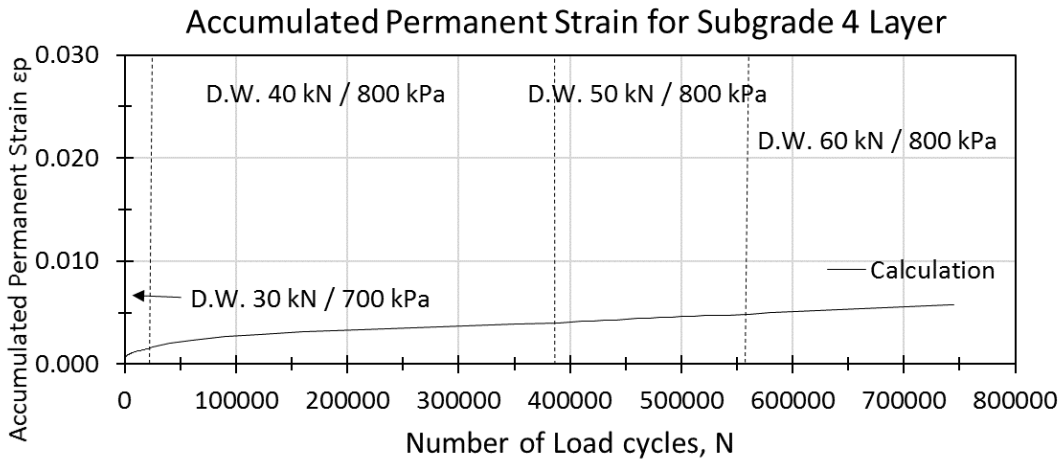

Figure 4.35 Accumulated permanent strain for subgrade 4 layer, structure SE20.

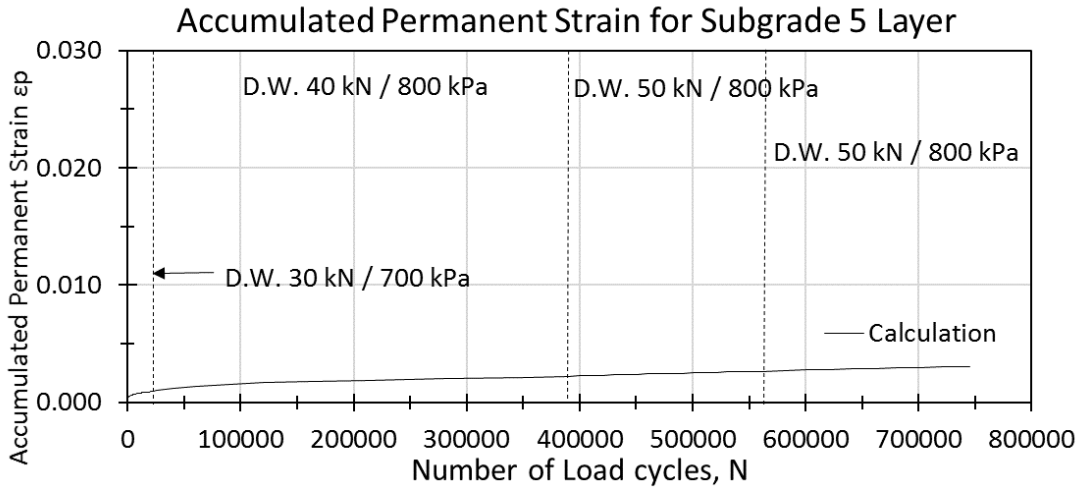

Figure 4.36 Accumulated permanent strain for subgrade 5 layer, structure SE20.

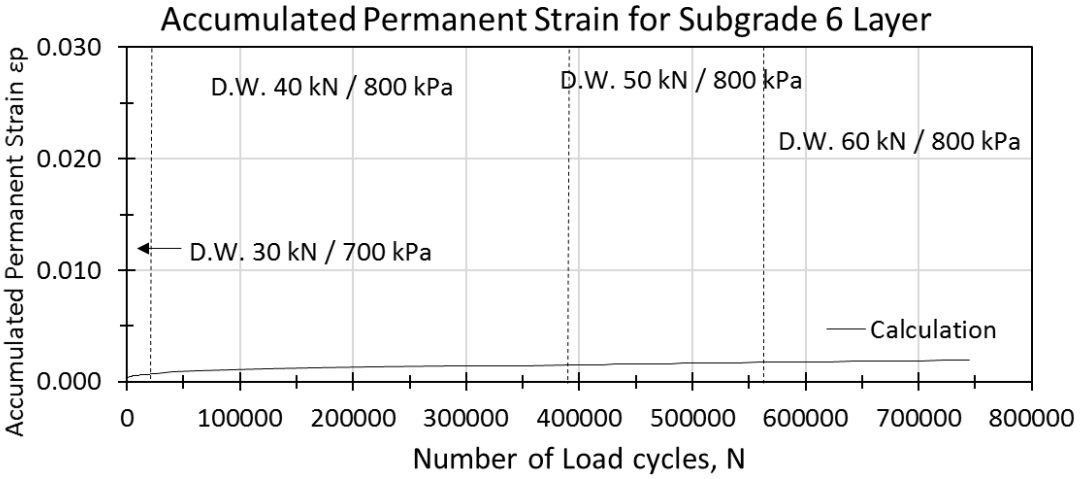

Figure 4.37 Accumulated permanent strain for subgrade 6 layer, structure SE20.

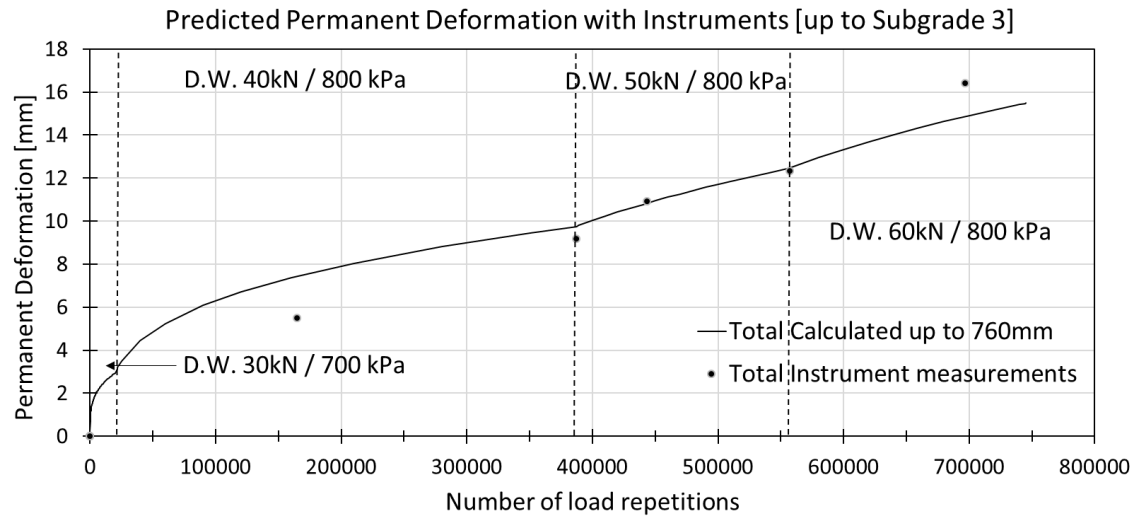

Figure 4.38 Predicted permanent deformation with instrument, structure SE20.

Good correlations are found for Figures 4.38 and 4.39, when comparing the profile measurements and the calculated models.

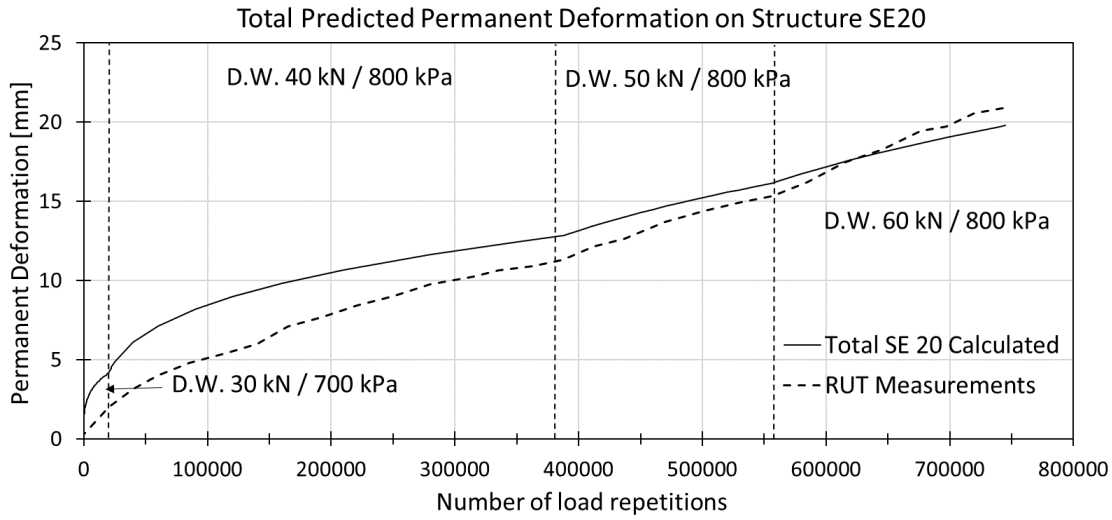

Figure 4.39 Total predicted permanent deformation on structure SE20.

For the SE20 structure of 196 cm, the total permanent deformation predicted at 800000 load repetitions is 20 mm. The analysed model over-predicts the deformation values at the beginning of the load repetition, but provides good agreement at 800000 load repetition, same as for structure SE18.

4.4.3 Estimated permanent deformation on SE14 structure

The initial vertical displacement data from the εMU coils obtained from VTI for structure SE14 was not of good quality, thus the values shown below are based on test results from SE18 and SE20.

4.4.3.1 Asphalt layer

Equation (12) was used for the PD of the asphalt layer. The values used for equation (12) are given in Table 4.10.

Table 4.10 Asphalt model parameters for structure SE14.

a_1 [-]	a_2 [-]	a_3 [-]	β_1 [-]
0.021	1.85	0.27	1.0

The asphalt layer for structure SE14 is ABT 16 and AG 32. The value assumed for the total asphalt layer structure is the same as SE18, i.e. a_1 = 0.021.

4.4.3.2 The unbound layer's model for SE14

Equation (10) was used for the prediction of the unbound layer. The value of *b* was kept constant for all the structures. The proposed *b* = 0.085 for SE14 shows good agreement when comparing the final rut. When comparing the degree of compaction E_{v1} and E_{v2} values of the base layer, SE14 is more compacted than SE18 and SE20 (Arvidsson, 2014).

The *a* values where kept the same as SE18, with the difference of subgrade 2, due to the different k_1 value found in Table 4.3. Additionally, it is expected that the lower layers are more compacted than the layers positioned above. The *a* values for subgrade 4 and 5 are half the previous layer. The time hardening or step load changes on the structure are after load repetitions 20000 and 600000 (Arvidsson, 2014).

The value of α is equal to 0.75, the same as with SE18 and SE20.

Table 4.11 Estimated model for unbound material SE14.

SE14	Thickness [cm]	*a* [-]	*b* [-]
Base	8.6	0.0012	0.085
Subbase 1	21.4	0.0004	0.085
Subbase 2	21.4	0.0002	0.085
Subgrade 1	15.0	0.00017	0.085
Subgrade 2	15.0	0.00034	0.085
Subgrade 3	35.0	0.00045	0.085
Subgrade 4	35.0	0.00022	0.085
Subgrade 5	35.0	0.00022	0.085
Total Layer	186.4		

In Figure 4.40, taking as an example D.W 40kN / 800kPa, dual wheel configuration with 40kN on half-axle load and a pressure of 800kPa is shown.

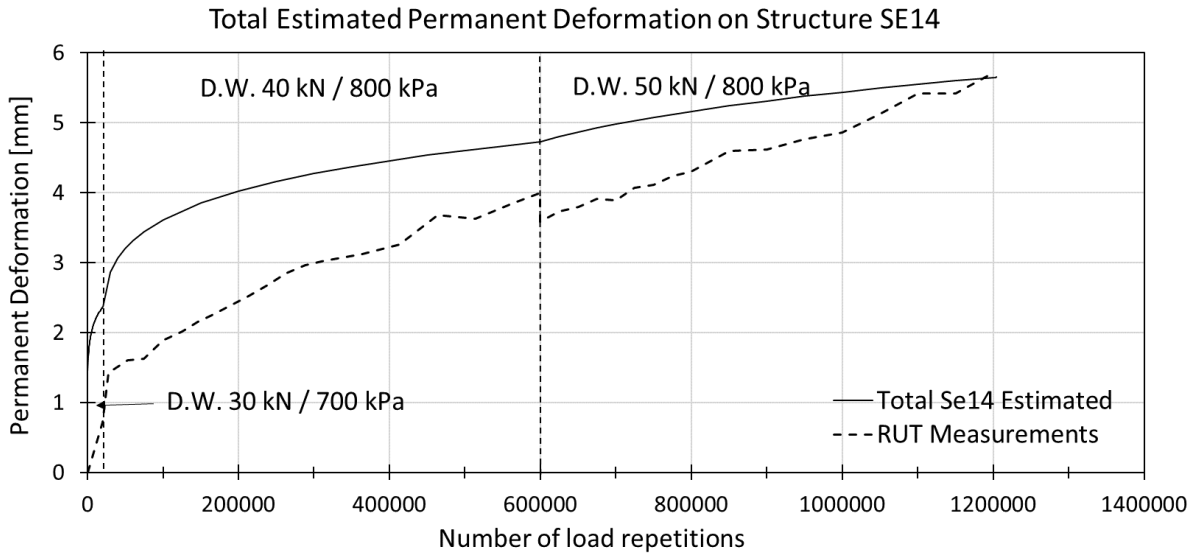

Figure 4.40 Total estimated permanent deformation on structure SE14.

The RUT measurements at load repetition 600000 shows inconsistent data, for this reason extrapolation is required. For a SE14 structure of 197.5 cm, the total permanent deformation at 120000 load repetitions is approximately 6 mm. Similar to SE18 and SE20, over-prediction is found at the beginning of the load repetition, but good correlation is found at the end of the load repetitions.

5 Conclusions, recommendations and areas for further study

5.1 Conclusions

A good pavement design should increase the life expectancy of the structure before its failure. To arrive in this prediction, it is important to know the main material parameters of the asphalt pavement structure. The Mechanistic-Empirical approach is very relevant in this thesis to attain, in accuracy the structural parameters of the models here proposed.

Structures SE14, SE18 and SE20 have been analysed in this study. All these three structures where built, instrumented, and tested with HVS in the APT facility in Sweden. An extensive amount of data was received from those structures for the validation of the M-E approach for predicting the rutting development of the structures. Additionally, the time hardening models proposed in this thesis show promising results of predicting the degradations of the SE14, SE18 and SE20 structures.

Major findings:

- The M-E methodology, the proposed parameters and the proposed models in this thesis can predict the rutting of all the test roads SE14, SE18 or SE20. The models and methodology are relatively easy to apply. Seasonal variables, traffic loading, and material types can be incorporated into the model to get realistic road life expectancy.

- For the response phase the asphalt bound layers and the subgrade material were modeled as linear elastic materials while the base and subbase were modelled as nonlinear stress dependent materials. Good agreement was found using those models between the three structures. This is true for the backcalculated FWD results as well as the wheel loading applied during the HVS-test.

- For predicting permanent deformation, the two simple models used here along with the time hardening approach to sum-up different load levels gave promising results when comparing measurements and calculations. The advantage of these two models is its simplicity because only a few material parameters are required.

5.2 Recommendations and areas of further study

The PD methodology proposed in this work can give an accurate prediction of rutting development of pavement structures and therefore save designers time, money and effort. An improved study of the key parameters *a* and *b* of the rutting models is needed with a bigger data base covering different types of materials of common use.

For the PD modelling of asphalt concrete layers, the values of the parameters a_1 *is* assumed based on the backcalculation. Additional laboratory tests are required for the asphalt layer ABT 16 and AG 32 to corroborate the values proposed here.

The instruments are located down to 80 cm of the total pavement structure. To have the total PD of the structure, instruments should be installed down to the entire depth of the test pit.

It would be interesting to use the proposed models of this thesis in a real road design using the same methodology as here, and complete a real-time measurement of the PD for the next five years, to compare the models and make a final assessment of the models.

References

Ahmed, A. W. (2014). Mechanical-Empirical Modeling of Flexible Pavement Performance, Ph.D. thesis, School of Architecture and the Built Environment. KTH Royal Institute of Technology.

Ahmed, A. W. & Erlingsson, S. (2012). Modeling of flexible pavement structure behavior – comparisons with Heavy Vehicle Simulator measurements. In Harvey, J., Jones, D., Mateos, A. & Al-Qadi, I. (eds.) *Advances in Pavement Design through Full-scale Accelerated Pavement Testing*. CRC Press, Taylor & Francis Group, London, pp. 493-503.

Ahmed, A. W. & Erlingsson, S. (2013). Evaluation of permanent deformation models for unbound granular materials using accelerated pavement tests. *Road Materials and Pavement Design*. 14/1, 178-195. doi:10.1080/14680629.2012.755936.

Ahmed, A. W. & Erlingsson, S., (2014). Evaluation of permanent deformations model for asphalt concrete mixtures using extra-large wheel-tracking and heavy vehicle simulator. *Road Materials and Pavement design*. 16:1, 154-171, doi:10.1080/14680629.2014.987311.

ARA Inc. (2004). "*Guide for the Mechanistic-Empirical Design of New and Rehabilitated Pavement Structures, Final report, NCHRP 1-37A.*" Transportation Research Board of the National Academies, Washington, D.C., USA.

Arvidsson, H. (2014). *HVS-test för skattning av nedbrytningseffekter från den tunga trafikens belastning; HVS-Nordic tests at VTI Sweden 2014. VTI report 35-2014,* Sweden: Swedish National Road and Transport Research Institute.

Das, B. (2002) Principles of Geotechnical Engineer. Fifth Edition. Sacramento: Wadsworth Group, 589 p.

Dawson, A. & Wellner, F. (1999). *Plastic Behavior of Granular Materials.* Final Report ARC Project 993, Reference PRG99014, April, 1999. The University of Nottingham.

Dynatest (2014), In-situ pavement stress and strain measuring transducers.

Doré, G. & Zubeck, H. K. (2009). *Cold Regions Pavement Engineering*. 1st ed. American Society of Civil Engineers, 1801 Alexander Bell Drive, Reston, USA.

Erlingsson, S. (2007). Numerical modelling of thin pavements behavior in accelerated HVS tests. *Road Materials and Pavement Design*. 8/4, 719-744.

Erlingsson, S. (2010a). Impact of water on the response and performance of a pavement structure in an accelerated test. *Road Materials and Pavement Design*. 11/4, 863-880. doi: 10.1080/14680629.2010.9690310.

Erlingsson, S. (2010b). Pavement Performance Models (NordFou-PPM). *Nordic Cooperation Program*. Report no. 2.4.1.

Erlingsson, S. (2012). Rutting development in a flexible pavement structure. *Road Materials and Pavement Design*. 13/2, 218-234. doi:10.1080/14680629.2012.682383.

Erlingsson, S. & Ahmed, A. W. (2012). ERAPAVE user's manual. *Swedish Road and Transportation Research Institute, VTI.*

Geokon (2013). Instruction Manual, Model 3500, 3510, 3515, 3600 earth pressure cells, Geokon, Inc. Lebanon, New Hampshire, USA

Lekarp, F., (1999). Resilient and Permanent Deformation Behavior of Unbound aggregates under Repeated Loading. Doctoral Thesis. Royal Institute of Technology (KTH), Stockholm Sweden.

Lekarp, F., Isacsson, U. & Dawson, A. (2000a). State of the art. I: Resilient response of unbound aggregates. *Journal of Transportation Engineering, ASCE*. 126/1, 66-75.

Lekarp, F., Isacsson, U. & Dawson, A. (2000b). State of the art. II: Permanent strain response of unbound aggregates. *Journal of Transportation Engineering, ASCE*. 126/1, 76-83.

Lytton, R.L., Uzan J., Fernando, E. G., Roque, R., Hiltumen, D. & Stoffels, S. M. (1993). Development and validation of performance prediction models and specifications for asphalt binders and paving mixes. *The Strategic Highway Research Program Project Rep. No. SHRP-A-357.*

NCHRP (2004). *NCHRP synthesis 325 – Significant findings from full-scale accelerated pavement testing*. Transportation Research Board of the National Academies. Washington, D.C., USA. source: www.trb.org.

NTEC -Nottingham Transportation Engineering Centre-. (2013). Testing equipment. Taken from http://www.nottingham.ac.uk/research/groups/ntec/facilities/equipment.aspx

Mamlouk, M.S (2006). Design of flexible pavements. In T.F.Fwa (Ed.) The Handbook of Highway Engineering. Taylor & Francis Group, Boca Raton, USA, pp. 8.1-8.34.

Oscarsson, E. (2007). Predicting of Permanent Deformations in Asphalt Concrete Using the Mechanical-Empirical Pavement Design Guide. *Department of Technology and Society Lund University; ISSN 1653-1930.*

Oscarsson, E. (2011). Evaluation of the Mechanistic-Empirical Pavement Design Guide model for permanent deformations in asphalt concrete. *International Journal of Pavement Engineering*, 12/1, 1-12. doi:10.1080/102984 30903578952.

Rahman, M. S. (2014). *Characterizing the Deformation Behaviour of Unbound Granular Materials in Pavement Structures*. Pd.D. Thesis, Stockholm: KTH, Royal Institute of Technology, Sweden.

Rahman, M. S. & Erlingsson, S., (2013). Moisture sensitivity of the Deformation Properties of Unbound Granular Materials. *Proceedings of the 9th International Conference on Bearing Capacity of Roads and Airfields, BCRRA'13,* Trondheim, Norway, pp 777-786.

Rahman, M. S. & Erlingsson, S., (2014). Evaluation of permanent deformations characteristics of unbound granular materials from multi-stage repeated load triaxial test. In compendium of papers of the 92nd Annual Meeting of the Transportation Research Board, Transportation Research board of the National Academies, Washington, D.C., January, 2014.

Rahman, M. S. & Erlingsson, S., (2015). A Model for predicting permanent deformation of Unbounded Granular Materials. Road Materials and Pavement Design, Vol. 16/3, pp. 653-673, doi:10.1080/14680629.2015.1026382.

Saevarsdottir, Th. (2014). Performance Modelling of flexible Pavements Tested in a Heavy Vehicle Simulator. Ph.D., thesis, Faculty of Civil Environmental Engineering, University of Iceland, Iceland.

Saevarsdottir, Th. & Erlingsson, S. (2012). Evaluation of Flexible Pavement Structure in an Accelerated Pavement Test. In Harvey, J., Jones, D., Mateos, A. & Al-Qadi, I. (eds.) *Advances in Pavement Design through Full-scale Accelerated Pavement Testing*. Taylor & Francis Group, London, pp. 237-248.

Saevarsdottir, Th. & Erlingsson, S. (2013a). Water impact on the behaviour of flexible pavement structures in an accelerated test. *Road Materials and Pavement Design*. 14/2, 256-277. doi: 10.1080/14680629.2013.779308.

Saevarsdottir, Th. & Erlingsson, S. (2013b). Effect of moisture content on pavement behaviour in a heavy vehicle simulator test. *Road Materials and Pavement Design*. 14/1, Special Issue EATA 2013, 274-286. doi:10.1080/14680629.2013.774762.

Saevarsdottir, Th. & Erlingsson, S. (2015). Modelling of responses and rutting profile of a flexible pavement structure in an HVS test. *Road Materials and Pavement Design.* Vol. 1b/1, pp. 1-18. doi: 10.1080/14680629.2014.939698.

Saevarsdottir, Th., Erlingsson, S. & Carlsson, H. (2015). Instrumentation and performance modelling of Heavy Vehicle Simulator Tests. *International Journal of Pavement Engineering*. 17:2, pp.148-165. doi: 10.1080/10298436.2014.972957.

Said, S. F., Hakim, H., & Oscarsson, E (2013). Rheological characterization of asphalt concrete using a shear box. Journal of Testing and Evaluation, Vol. 41 No. 4, pp 602-610, doi: 10.1520/JTE20120177. ISSN 0090-3973.

Sweere, G. T. H. (1990). *Unbound granular bases for roads*. Ph.D. thesis, Delft University of Technology, Netherlands.

Werkmeister, S., Dawson, A. R. & Wellner, F. (2001). Permanent Deformation Behaviour of Granular Materials and the Shakedown Concept. *Transport Research Record, Journal of the Transportation Research Board (TRB) No. 1757,75-81*.

Wiman, L. G. (2006)., *Accelerated load testing of pavements; HVS-Nordic tests at VTI Sweden 2003-2004. VTI rapport 544A* Swedish National Road and Transport Research Institute. Sweden.

Wiman L. G. & Erlingsson S. (2008), "Accelerated pavement testing by HVS – a transnational testing equipment", *Transport Research Arena Europe 2008*, Ljubljana, 21-24 April, 2008, CD ROM.